Chapter 4
The Structure of Metals and Alloys

4.1 The World of Microstructure and Phase Diagrams

The properties of metals and alloys are dependent on their atomic structure. Metals are an aggregation of atoms that, apart from mercury, are solid at room temperature. These atoms are held together by "metallic bonds" that result from sharing available electrons. A negative electron bond pervades the structure, and heat and electricity can be conducted through the metal by the free movement of electrons. The atoms are regularly arranged, forming a symmetrical three-dimensional group, which repeats itself periodically and which is called a unit cell. Unit cells of identical characteristics form a crystal with regular spatial distribution of atoms, which can be defined by a space lattice. Atoms can be stacked in different ways to create a variety of simple lattice types. There are three common types of lattice structure that most metals belong to (Fig. 4.1): face-centred cubic (fcc), body-centred cubic (bcc) and close-packed hexagonal (cph).

In the face-centred cubic (fcc) lattice, layers of atoms can be built up, which can be modelled in spheres, so that the third row of spheres does not occupy the same position as the spheres in the first row; the structure then repeats every third layer (ABCABCABC…). In the close-packed hexagonal structure (cph), a model can be made up of spheres stacked in layers as well, but in the hexagonal structure, the spheres repeat the pattern every second layer (ABABABAB…). In the body-centred cubic metals (bcc), the atoms are arranged at the corners of a cube with one atom in the centre of the cube.

This arrangement is strong but allows substitution of solvent atoms by atoms of a solute or other atoms to enter the cube if they have small radii, such as carbon or nitrogen in steels. The latter are called interstitials, because they fit between the interstices of the lattice of a solvent and expand the unit cell of the solvent. There are only a few elements such as hydrogen, carbon, nitrogen or boron, with radii small enough, capable to locate between the atoms of a solvent (H = 0.037 nm; B = 0.082 nm, C = 0.077 nm; N = 0.071 nm). The ability of carbon, in particular, to

© Springer Nature Switzerland AG 2019

D. A. Scott, R. Schwab, *Metallography in Archaeology and Art*, Cultural Heritage Science, https://doi.org/10.1007/978-3-030-11265-3_4

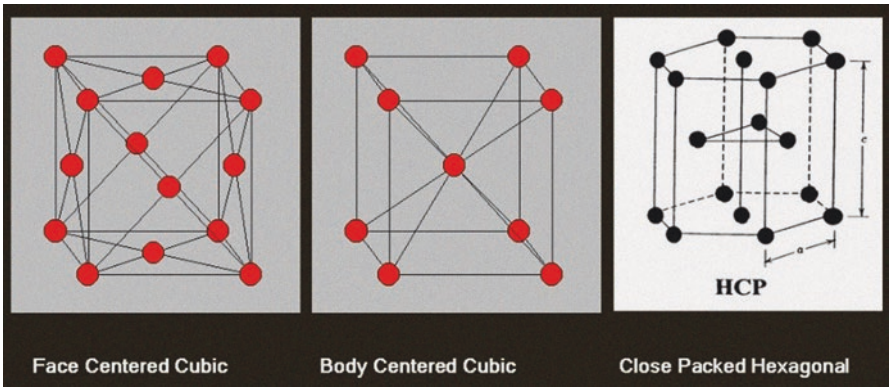

Fig. 4.1 Unit cells of the three common space lattices in ancient metals and their arrangement of atoms

fit into the iron lattice produces steels, which have considerable strength, compared with pure iron.

More important and more common is the replacement (substitution) of solvent atoms by those of the solute, which has been regarded by the traditional chemical view of early researchers as a solid solution of one metal in the other. The term solid solution is used when atoms of different elements are able to share the same phase together, that is, when solute atoms are soluble within the crystal lattice of a solvent without changing the type of structure of the host metal. Atomic size, crystal structure and lattice parameters, chemical affinity and electron concentration are the factors governing solid solubility, whereas binding energy and specific gravity affect liquid miscibility or immiscibility. Actually, the degree of substitutional solid solubility of metal compounds, formed by different metals, is dependent on general factors that Hume-Rothery and co-workers determined by their experimental work on several metallic systems (see, e.g. Hume-Rothery and Raynor [41]). Those "Hume-Rothery Rules" predict that metals must have the same type of lattice structure for complete solid solubility, that the difference between atomic sizes of alloying elements must not exceed 15%, that the chemical affinity should not be high and when the ratios of valence electrons to atoms are different and that the lower valance metals have better solubility than vice versa. Deviation from Hume-Rothery's Rules leads to a decrease in the maximum solid solubility and finally to immiscibility or to a tendency to form other compounds, such as intermetallic phases, rather than solid solutions. The atomic size difference between solvent and solute is generally always a parameter of the extent of solid solution strengthening. In fact, there exist several aberrations from these rules, and we recommend the reader who is interested to consult some of the original work for evaluating the general concepts (e.g. Hume-Rothery and Raynor [41]) and some critical interpretations (e.g. Barrett and Massalski [5]; Mizutani et al. [72]; Zhang et al. [131]).

One of the most useful theoretical aids to the study of the microstructure of ancient metals is the equilibrium diagram, also called the phase diagram or consti-

tutional diagram. Since many alloys are mixtures of two, three or more different components, phase diagrams are used to plot temperature against composition and to map out the areas of the different phases, which occur at different compositions or temperatures in the system concerned.

All standard phase diagrams refer to a fixed pressure of constant atmosphere. Phase diagrams provide information about melting and freezing temperatures, solubility limits and phase stability under conditions of equilibrium. The emphasis is on equilibrium conditions, which is an important parameter to remember. Phase diagrams are valid only when components achieve equilibrium conditions, which almost never occurs completely in ancient metals. This means that the interpretation of the microstructure of some metallic systems has to be carried out with care and with an awareness that the system might not be in equilibrium.

If there is some reason why this ideal state cannot be reached, then the actual microstructure which is observed in ancient artefacts will be potentially different from that predicted by the phase diagram. The phase diagram is, however, the essential skeleton on which the details of the appearance of the system hang, even if the ancient alloys in question are far removed from an equilibrated state. Nevertheless it is possible to predict phases that are present in the microstructure with their chemical composition and their amounts in alloys approximately to the compositions shown in the diagrams in many instances, especially in worked and annealed alloys. It is in cast alloys that the general relationship between phase diagrams and the proportion and composition of the phases predicted by them tends to break down.

A phase is a component of an alloy system whose composition can vary within certain limits or have a fixed stoichiometric ratio of different kinds of atoms. As a result, phases can be of rather variable elemental composition, for example, the alpha phase in the copper-tin system, which is the copper-rich primary solid solution (α_{Cu}), could have less than 1% of tin or up to a maximum of 15.8% of tin dissolved. It could not have 20% of tin, because that is outside of the stability limits of the alpha phase and another phase will replace the alpha phase. The delta phase in the copper-tin system, which is an intermetallic compound, has a fixed stoichiometric ratio of $Cu_{41}Sn_{11}$ with 32.55% tin instead [98]. Indeed several earlier researchers found that the delta phase would be of slightly variable composition at different temperatures but corresponding to the formula $Cu_{31}Sn_8$, which has been the long-established stoichiometric formula (see Hansen and Anderko [35] for critical evaluations of the literature).

More recent compilations of the data and thermodynamic assessment indicate that the ideal formula would be $Cu_{41}Sn_{11}$ [98, 107]. The delta phase would have a very limited thermodynamic stability under equilibrium conditions, but the cooling rate is the most decisive factor that affects the decomposition of the delta phase, and in practice, the delta phase is stable and persists for thousands of years without change.

As a result, the copper-tin system can be redrawn at lower tin concentrations to create phase diagrams, which actually relate to empirical conditions rather than thermodynamic theory that will be given later in Chap. 5.

Alloys do not have a particular melting point. They soften and pass through a pasty stage between temperature zones shown on the phase diagram as solidus and liquidus curves. The solidus is the line in the phase diagram that separates the pasty stage of the alloy, usually a mixture of solid and liquid, from the completely solid alloy below the temperature of the solidus line. The liquidus is the line on a phase diagram that shows the temperature at which solidification begins on cooling from the melt.

The boundary region between these lines can be narrow or broad. In some alloys of importance in antiquity, such as copper-tin, gold-copper-silver or copper-arsenic, there is considerable separation between liquidus and solidus curves, which exacerbates the difficulties of attaining equilibrium cooling conditions from the melt and enhances the segregation effects that can be observed in these alloys. This is because the alloy has a longer period of time in a semi-solid region of partial solidification in which time for segregation to become fixed in the solid is accentuated compared with alloys with a narrow separation between liquidus and solidus. It is especially prevalent in copper-arsenic alloys, which have a steep and broad incline in the liquidus area at low arsenic concentrations, and consequently segregation can be severe.

Conventional binary phase diagrams are two-dimensional plots of the two components on each end of the horizontal axe versus the temperature on the vertical axe. The compositions of the solute and the solvent are given in atomic percent and in weight percent on the abscissae, whereas temperature is usually given in degree Celsius, and additionally, but less common in more recent publications, in degree Fahrenheit, on the ordinate. Some American publications persist in using degrees Fahrenheit, particularly in the iron and blacksmithing fraternity, which can be very confusing, as the temperature scale they are referring to is frequently not mentioned, or not defined, in the publication concerned.

Greek letters such as α, β, μ, δ, etc. are customarily used in order of their appearance – ordinarily upon cooling and increasing solute concentration but with arbitrary exceptions – to designate crystalline phases in metallic systems. Unfortunately phase designations are not used consistently, and there are several serious confusions in terminology, for example, with a particular Greek letter meaning one phase in one binary system and a different phase in another, or phases having the same crystal structure are labelled with different letters.

Complications caused by the labelling of the phase diagrams have been mitigated by employing stoichiometric formula instead, together with retaining established traditional phase names, which can be somewhat confusing, and with more complex alloy systems can become very annoying. Nevertheless, there are a few general conventions: solid solutions should be designated by the chemical symbol of the base element as subscript and a Greek letter additionally; disordered body-centred cubic structures are usually labelled with β (β’ for ordered) or γ for brass-type structures (e.g. Hansen and Anderko [35]; Chang et al. [17]; Massalski [63]). The region of the liquidus is labelled *L,* whereas the labelling of the solid phases with *S* will only be used in the following to discuss general reactions.

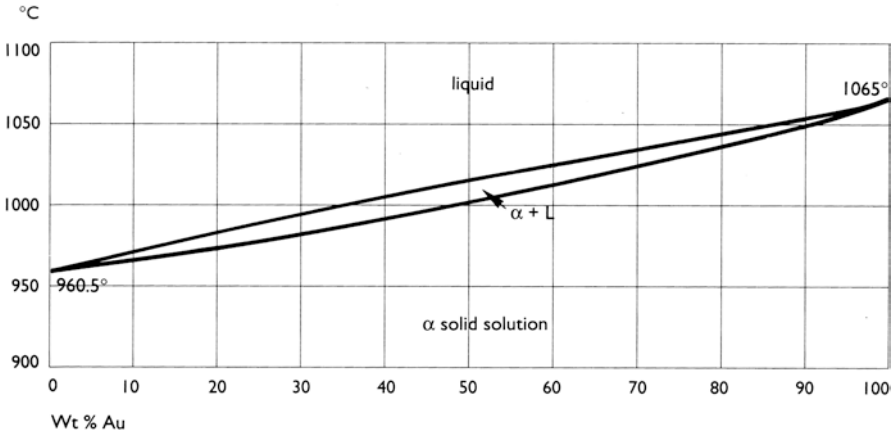

Fig. 4.2 The gold-silver equilibrium diagram

All metals show some solubility in the solid state but in very different proportions. Some metals are completely soluble in each other, and the easiest systems of this class are so-called isomorphous systems, because of the complete liquid and solid miscibility of two elements and a single-phase solid solution which forms for all alloy compositions in the solid state. The phase diagram for the gold-silver system which is a good example is shown in Fig. 4.2.

Gold and silver have the same cubic face-centred (fcc) crystal structure, with very small differences in their lattice constants and their atomic radii (Au = 0.1442 nm; Ag = 0.1444 nm). At any composition of the alloy as it cools down, it reaches the liquidus line and begins to solidify, until the solidus line is reached, at which point the entire alloy is a solid mass of crystals. This is a completely homogeneous solid solution shown on the diagram as the alpha phase, and the grains are usually close to their equilibrium predicted state. The gold-silver system in which complete solid solubility occurs between two components is actually uncommon: most metallic elements are not completely soluble in each other, and at different compositions, different phases form, and these can be seen in the polished and etched microstructures and are modelled by the equilibrium constraints affecting their composition and temperature stability.

Another simple system, but the least common form of binary phase diagram and totally different to the isomorphous systems, are systems with nearly no miscibility in the liquid nor in the solid state. Iron and lead is the best-known so-called monotectic system that has some relevance in ancient metallurgy (Fig. 4.3). In the melt, iron and lead separate due to their different specific gravity, so that the lighter iron solidifies on top of the liquid lead ($L \leftrightarrow S_{Fe} + L_{Pb}$) and finally two layers of solid iron and solid lead remain.

Much more important for many metallurgical processes, such as the so-called cupellation and liquation processes (Sect. 5.1.2), is a three-phase reaction; the monotectic reaction takes place when one liquid phase decomposes with decreasing

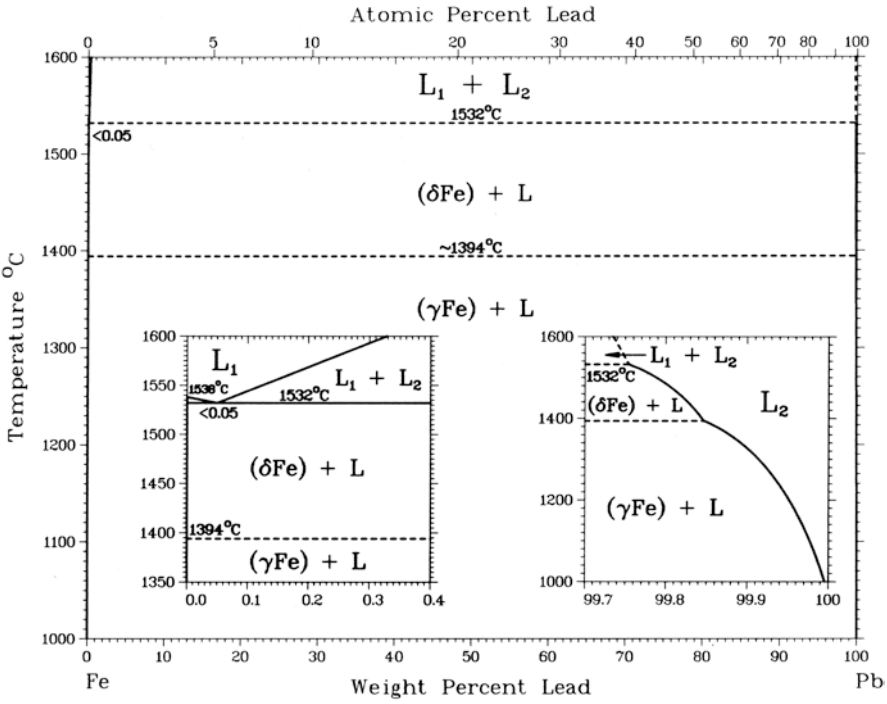

Fig. 4.3 Iron-lead monotectic-type equilibrium diagram. (From Massalski [63])

temperature into a solid phase and a new liquid phase of different composition is formed.

Some phase diagrams of monotectic alloys, such as copper and lead, shown in Fig. 4.4 contains a liquid miscibility gap, in which two liquid phases coexist over a certain composition range and finally constitute individual solid phases of copper and lead ($L_{Cu} + L_{Pb} \leftrightarrow S_{Cu} + S_{Pb}$).

Liquid copper and liquid lead are completely soluble in each other at high temperatures, but with higher lead percentages, between 36% and 87%, lead separates into two liquids on further cooling. Actually, the composition of a copper-lead alloy does not need to be within that range for the monotectic reaction to occur. During freezing of lead-rich copper-lead alloys, the copper-rich α_{Cu}-phase forms first, and the composition of the melt shifts towards the monotectic composition and decomposes. Both solids have only a very limited solubility for each other, and the microstructure of copper-lead alloys usually shows randomly distributed lead particles within a α_{Cu}-matrix. An example is shown in Fig. 4.5.

The fact that lead enters into these reactions with copper at higher temperatures helps to prevent the gross separation of lead from copper, and instead, the most common distribution is in the form of small globules or droplets of lead scattered throughout the object.

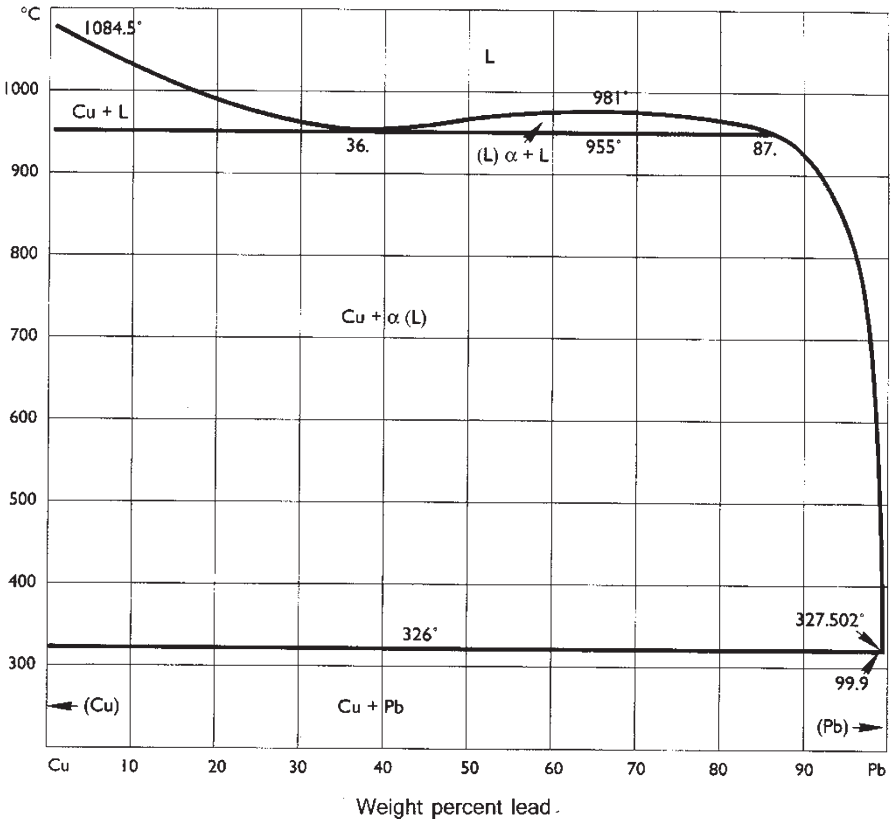

Fig. 4.4 The copper-lead phase diagram with miscibility gap

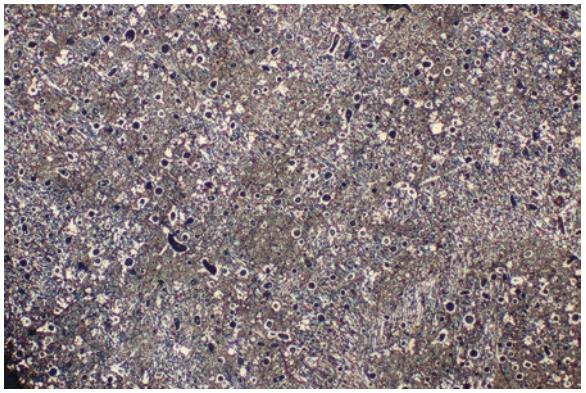

Fig. 4.5 Distribution of fine lead droplets in the ideal cast Chinese bronze mirror from the Han dynasty. The fine lead precipitation ensures that an even and highly reflective surface can be obtained from the mirror, of classic Chinese composition, 5% lead, 25% tin and 70% copper. Etched in ferric chloride, magnification ×200

The lack of solubility of lead in copper has been used in the past to de-silver copper-silver alloys. A cake of the silver-bearing copper is cast into a large disc with the addition of lead. On cooling the discs are held vertically in a furnace, and the lead is molten out by slow heating, leaving a porous copper cake behind, but as silver is attracted to the lead, the molten lead can be cupelled to remove the silver and can be smelted back to metallic lead again, allowing the whole process to be repeated with a new cake of copper, producing metallic silver as a useful by-product (see Chap. 5).

One of the most common types of equilibrium diagrams is that which includes a eutectic, a mixture of two phases in close spatial proximity, which microstructure is usually lamellar, shown in Fig. 4.6, or globular, as in Fig. 4.7.

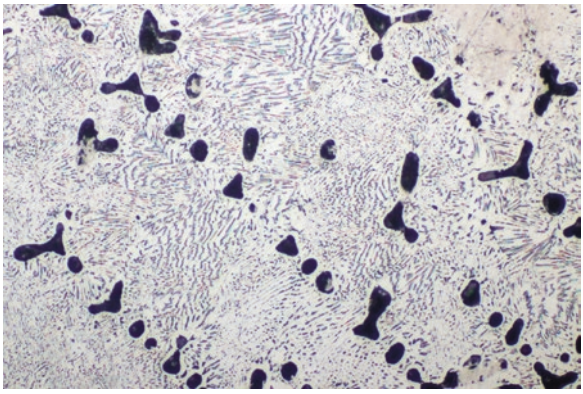

Fig. 4.6 60Ag40Cu alloy as cast. The alloy will precipitate copper-rich dendrites with an infill of the $\alpha_{Ag} + \alpha_{Cu}$ eutectic. As shown here, the eutectic is lamellar, with a fine spacing between the two phases which make up the eutectic. According to the phase diagram, the α_{Cu} dendrites should have about 8% silver content, as a heavily segregated alloy system, this value did not change on cooling, a fact confirmed by electron microprobe analysis. Etched in ferric chloride with nitric acid, magnification ×220

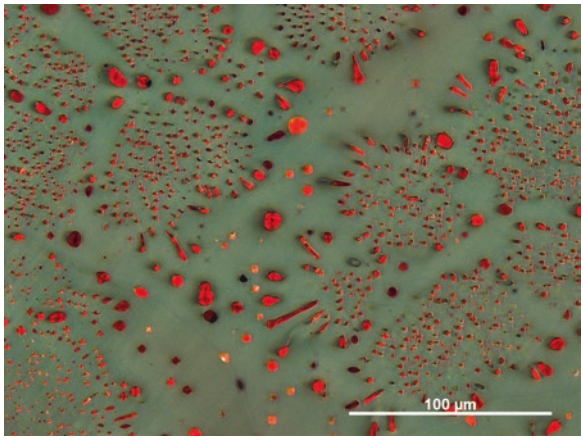

Fig. 4.7 Microstructure of a dealloyed and partly oxidized casting waste from the oppidum of Manching, showing globular microstructure of Cu-Cu_2O eutectic viewed with crossed polarized light

Simple binary eutectic systems are characterized by a solid-solid miscibility gap and have their minimum melting temperature at the eutectic point, when three phases are at equilibrium. The eutectic reaction converts one liquid phase directly into two distinct solid phases: $L \leftrightarrow S_\alpha + S_\beta$. The silver-copper system, which is shown in Fig. 4.8, is of timeless importance, as silver-copper alloys have a very long history (Chap. 5).

The area above the liquidus line shows the region where the mixture is liquid and the areas between liquidus and solidus line, where the alloy is a mixture of liquid and solid phases. The region below the eutectic isotherm is a mixture of two solid phases, a face-centred cubic silver-rich solid solution on the left side, here labelled α_{Ag}, or simple designated as (Ag), and a copper-rich solid solution of the right side. A typical range of microstructural types is shown in Fig. 4.9.

Due to traditional labelling, this phase is usually called β, whereas it is also face-centred cubic and is therefore sometimes labelled α_{Cu} or simply designated as (Cu). At the eutectic point, the molten alloy passes directly from liquid to solid, at 71.9% silver and 28.1% copper. Notice that the melting point of the eutectic is much lower than the melting point of either of the pure constituents, at 779 ° C. This is of great practical importance, since silver artefacts can then be soldered together with silver-rich alloys without the danger of the silver artefact itself becoming molten.

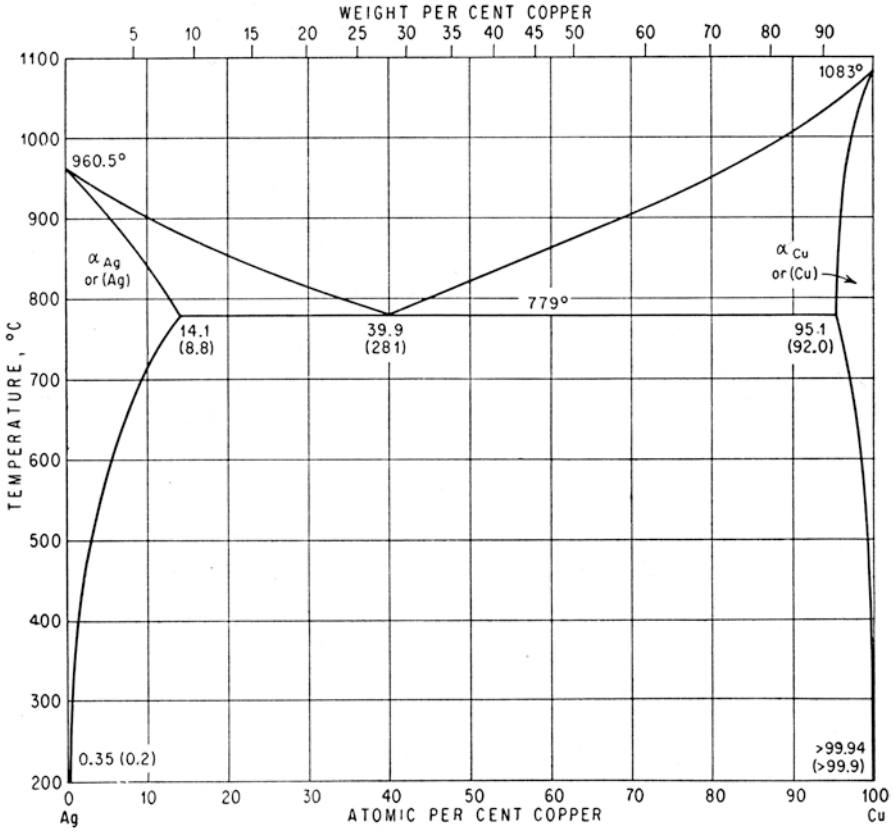

Fig. 4.8 The silver-copper phase diagram (after Hansen and Anderko [35])

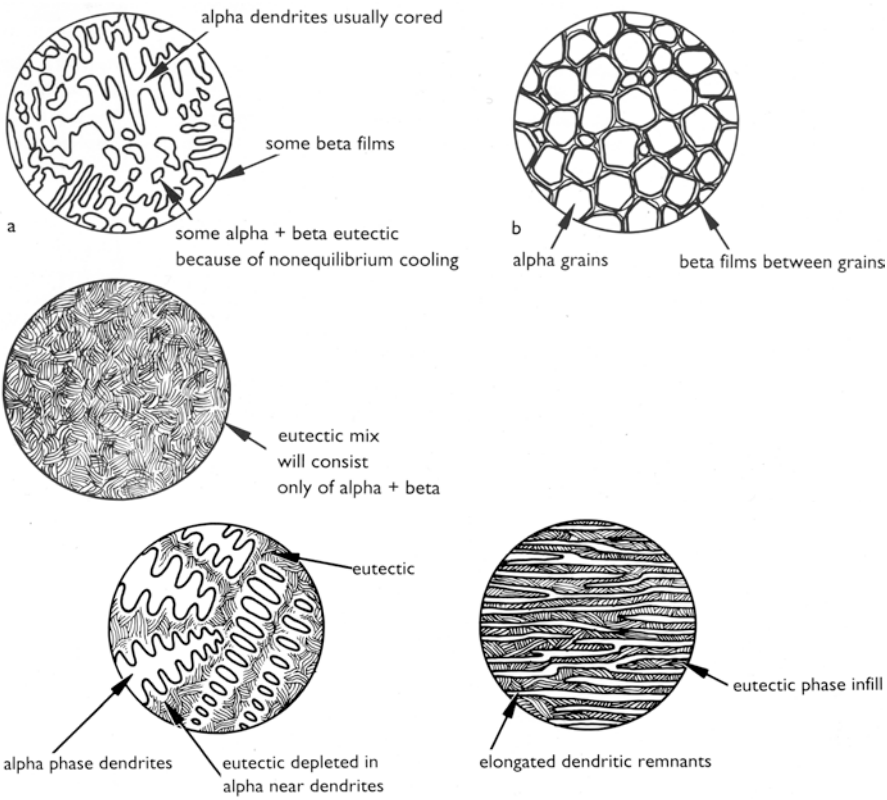

Fig. 4.9 Range of microstructural types of Ag-Cu alloys (after Scott [103])

Equilibrium is very sluggish in the silver-copper system, and in some alloys, very little change in composition of the cast phases takes place from the period of their solidification to their worked end product. Microstructures of alloys with compositions less than the eutectic are termed hypoeutectic and hypereutectic when greater than the eutectic composition. For alloys with a solid-to-solid transition, the phrases used are hypoeutectoid and hypereutectoid.

For soldering in precious metals, various proportions of copper and silver are used for this kind of operation, and a number of different recipes are recommended by classical recipes, such as those described by the Renaissance craftsman, Benvenuto Cellini [15, p. 93]: "…the solder I used was *ottavo*, that is a solder composed of one-eighth part of an ounce of copper to one of silver…….I bound the two legs to the body. Then I laid it on the wall over a good fire, and applied *quinto* to it, i.e., solder composed of one fifth of an ounce of copper to one of silver. As I worked with eleven-and-a-half silver to half copper I had nothing to fear as far as the latter was concerned and I would have everyone aware that if he wishes to make his job succeed he must not employ inferior silver…".

The statue that Cellini was working on was therefore cast in an alloy of 99.6% silver and 0.35% copper [15, 104]. This is practically pure silver with a melting

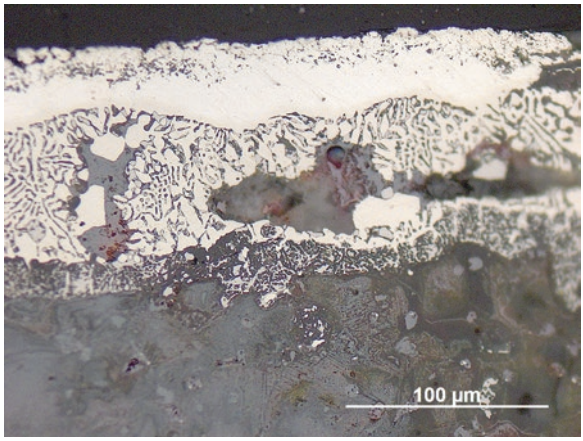

Fig. 4.10 Unetched microstructure of a soft-soldered silver sheet on a bronze surface viewed with bright-field illumination. The micrograph shows Ag_3Sn-Cu_3Sn eutectic between sheet and substrate, in which copper-rich phases are partly corroded

point of 961 °C. The ottavo solder has a composition of 91.1% silver and 9.9% copper, with a liquidus of 880 °C, while the quinto solder, used for heavier attachments, has a composition of 86.1% silver and 13.9% copper and has a liquidus at 845 °C. All of these alloys are hypereutectic and will precipitate silver-rich phases first during solidification. The phase diagram shows that the quinto alloy melts at a temperature over 100 °C less than that of the silver Cellini used for the statue itself.

Another important eutectic alloy in antiquity is that of the lead-tin system which produces a range of microstructures rather similar to that of the copper-silver system. The eutectic point of the lead-tin system, for example, is relevant to soft solders, which have been used from archaic Greece to modern times (Chap. 5). Eutectic points of several systems have usually no technological relevance to most customary pre-industrial alloys, but their phase diagrams are important in the interpretation of some unusual microstructures, which might have been produced accidentally, like that shown in Fig. 4.10 that shows a cross section of a fragment coming from a life-sized Roman statue found in Luxembourg [28].

This fragment has been plated by a silver sheet, which has been soldered to the bronze body by a tin solder. The eutectic point of the Ag-Sn system is at 221 °C and 96.2 atomic percentages of tin, where the liquid would decompose into the silver-rich intermetallic ε-compound (Ag_3Sn) and β_{Sn} [47], but the newly formed tin-silver solder has reacted with the bronze and decomposed eutectically to silver-rich ε-phase (Ag_3Sn) – labelled θ in the ternary system – and tin-rich ε-phase (Cu_3Sn) of the Cu-Sn system – labelled ε_1 in the ternary system [17].

Figure 4.11 shows a generalized eutectic equilibrium diagram and some of the typical types of microstructure associated with eutectic alloys of metals A and B. Alloy of composition I is a hypoeutectic alloy, having less of component B than the eutectic. If cooled under equilibrium conditions, at point c on the diagram, solid begins to precipitate. This solid is a primary solid solution of B in A. As cooling proceeds, the composition of the solid moves along the solidus line, and the liquid cools until it reaches the point E at which it breaks down into the two different phases of alpha plus beta as a fine eutectic mixture. This is shown in drawing (a). Similarly if an alloy of composition II cools down, then grains of beta phase will

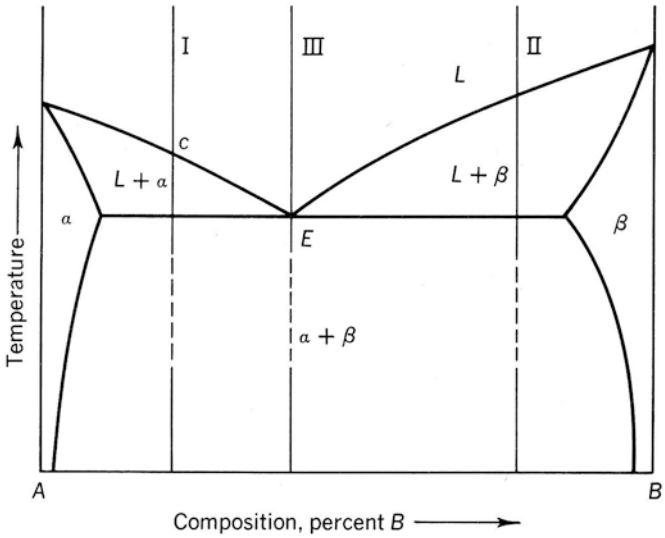

Phase diagram of the *A*-*B* system showing a typical simple eutectic diagram.

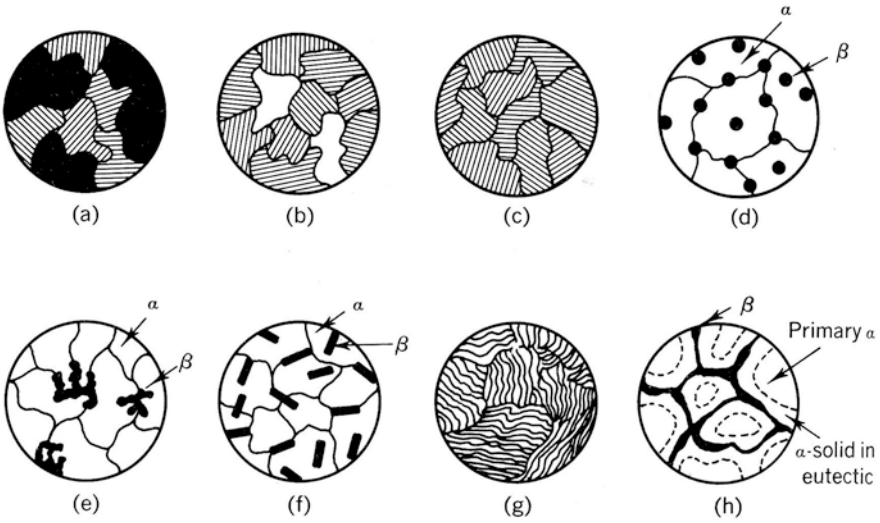

Fig. 4.11 Generalized eutectic equilibrium diagram and some of the typical types of microstructure associated with eutectic alloys of metals A and B

form, and the remaining infill will consist of the eutectic as shown in drawing (b). This alloy can be referred to as a hypereutectic, as it contains an excess of component B. Alloy III corresponds exactly to the eutectic point E and will pass directly from liquid to solid forming a fine intermixture of the eutectic as shown in drawing (c). If the eutectic composition is close to the composition of one of the phases mak-

ing up the eutectic, then a variety of different microstructures are possible. These structures are the nodular, often spheroidal, structures, shown in drawing (d), the irregular precipitates of drawing (e), acicular precipitates of drawing (f), coarse lamellae of drawing (g) and the divorced eutectic of drawing (h). There is a tendency for the two phases to separate into large regions so that there is considerable divergence from a normal eutectic structure. In the divorced eutectic, there is no distinctive boundary between the primary solid solution and the portion of the same solid solution in the eutectic.

A similar phase change to the eutectic decomposition is the so-called eutectoid reaction. The difference is the transformation of a solid phase into two other solid phases at a certain temperature: $S_\gamma \leftrightarrow S_\alpha + S_\beta$. Eutectoid transformations are best known from the copper-tin system and iron-carbon alloys (Sect. 4.6 and 5.2).

Some binary systems such as the copper-gold system, shown in Fig. 4.12, which have also the same type of lattice structure (fcc) do not show a distinct eutectic point but have a so-called congruent melting minimum, which is of great importance to ancient goldsmithing techniques, such as granulation. Congruently melting compounds melt or decompose like isomorphous systems to a single phase without compositional alteration as in the eutectic reaction but also at a definite temperature. The copper-gold system does have some complications, because ordered phases can form at certain compositions, which may create brittleness in gold alloys if they are not annealed correctly (Sect. 4.6).

The last of the basic schemes of binary phase diagrams is the peritectic equilibrium diagram. The peritectic reaction is characterized by a primary precipitation of a solid phase from the liquid, which is temporarily thermodynamically stable and in equilibrium with the melt. There are different mechanisms of peritectic reactions, but generally, the primary solid phase is metastable and persists only for a finite length of time, whereas below the peritectic temperature, a new solid phase is formed: $L + S_1 \leftrightarrow S_2$. "Pure" peritectic systems are less common and without significance to ancient alloys. Indeed some of the most important systems such as Cu-Sn or Cu-Zn show one or more peritectic reaction. Most binary systems of interest do not consist of only eutectic, monotectic or peritectic reactions but of combinations of the fundamental reactions described above (see Chap. 5).

4.2 Intermetallics

Isomorphous or eutectic systems result in the formation of one or two solid solutions of large variable composition, whereas in peritectic systems or more complex systems with peritectic reactions, intermediate phases occur, which have a finite stability. Intermediate phases often have structures which are different from the component elements, and some of them have only a narrow range of compositions, whereas others show an extended compositional stability range. Due to the restricted

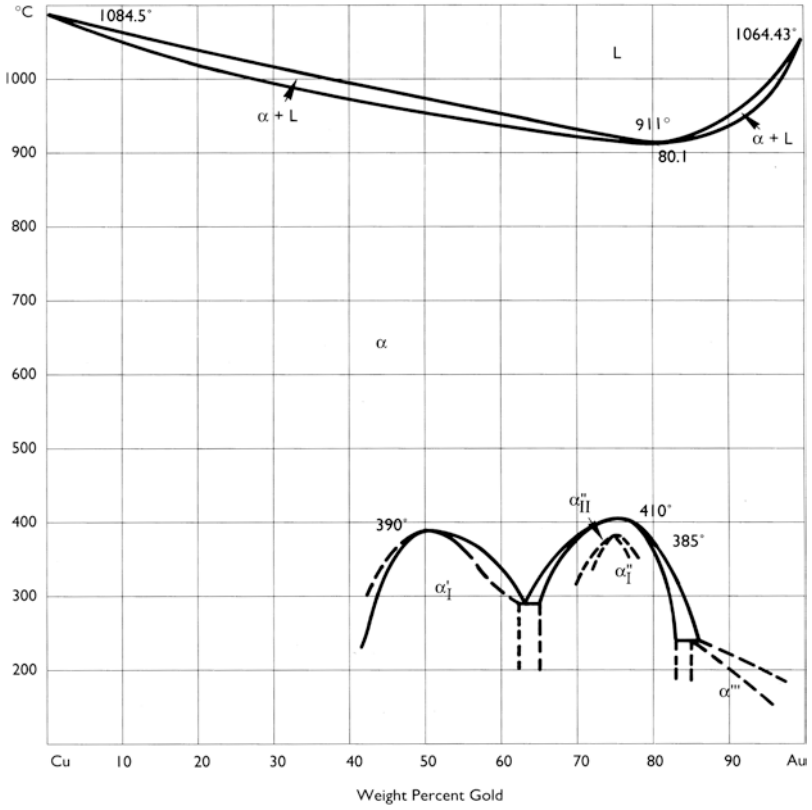

Fig. 4.12 Copper-gold equilibrium diagram

stoichiometric compositions of some intermediate phases, they are called intermetallic compounds. Modern physical metallurgical terminology differentiates between intermetallic compounds with sharply defined compositions and intermetallic phases with extended stability range and suggests using the term intermetallics for both (see Steurer [116]). Albeit their strict range of stoichiometry, intermetallic compounds do not obey normal valence rules, and their bonding is not only metallic (see Steurer [116]). The formation of intermetallics is relevant to many metallurgical processes and metalworking, since most intermetallics are much harder, have lower melting points and are more or sometimes less corrosion resistant than the solid solutions, and they usually have different colours. In consequence, the presence of intermetallics has significant influences on the mechanical, optical and casting properties of alloys. The formation of the δ-phase ($Cu_{41}Sn_{11}$) is not desirable in ancient bronzes, for example, on cold-working of alloys which contain the delta phase, because this phase tends to shatter when hammered, but the δ-phase is beneficial for reflectivity and polishing of special artefacts such as mirrors (Sect. 5.1). The presence of silver-coloured γ-phase (Cu_3As) on the surface of

objects made of arsenical copper has been discussed as being an intentional effect, which in some cases it may be, rather than due to inverse segregation. Silver-coloured copper alloys containing high amounts of tin, arsenic, antimony or nickel have been used in many cultures at different times to imitate silver (see Sect. 5.1). Beside nickel, the colour changes are all based on the presence of intermetallics.

4.3 Cast Structures

Inhomogeneity of metals is termed segregation. There are several forms of segregation. These are called normal, inverse and dendritic. Gravity segregation is usually not observed in ancient metals, although there are cases where lead has begun to pool to the bottom of some cast objects due to gravity, such as leaded bronze Roman mirrors. The most critical for copper alloys is dendritic segregation. An example is shown in Fig. 4.13.

As the liquid cools through the region where the first solid begins to form, small snowflake-like particles of solid begin to solidify. These are the dendrites. The dendritic structure is essentially affected by the cooling rate, which again depends on different factors such as elemental composition, size of the castings, mould material and temperature of the mould during casting as well as cooling rate. The spacing between adjacent arms in dendrites, so-called dendrite arm spacing (see Sect. 3.3.2.1), is made finer by increasing the cooling rate. Modern commercial copper alloys show minimum dendrite arm spacing of 10–100 µm [24], while small archaeological items have less than 10 µm.

Another common form of segregation produces columnar grains, long radiating crystals, which are usually seen in chill castings, copper ingots or copper electrotypes, and an example is illustrated in Fig. 4.14.

Chill castings are castings that have been made into an unheated mould. The columnar grains of chill castings are not very common in ancient cast materials,

Fig. 4.13 Casting dendritic segregation in a 20% tin 80% copper, tin bronze, air cooled from 1200 °C. Dendritic segregation results in the alpha + delta eutectoid structure being present between the alpha phase initial solidification. Etched in ferric chloride, polarized, magnification ×150

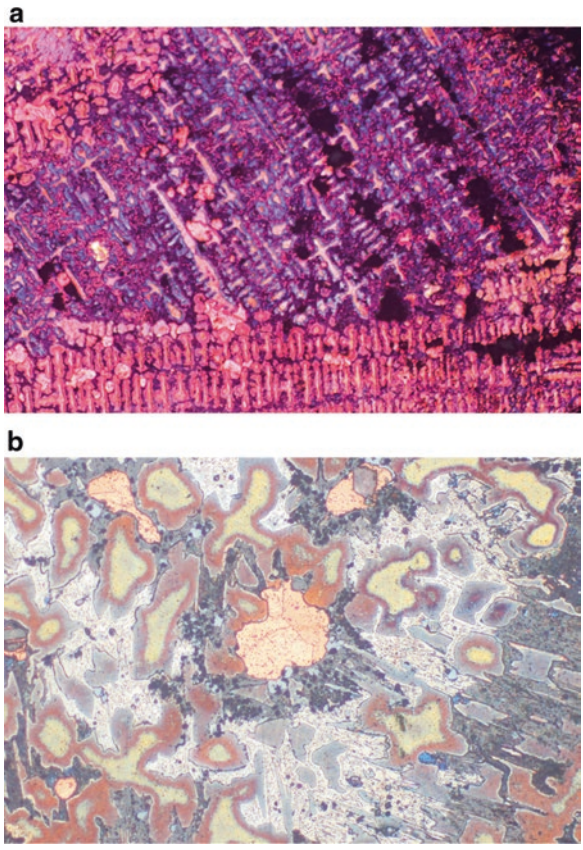

Fig. 4.14 (**a**) Luristan ceremonial dagger handle showing extensive coring and separation of the alpha + delta eutectoid, some of which has corroded, resulting in loss of tin and redeposition of metallic copper within the corroded matrix, clearly seen here. Colour etched in Klemm's reagent, magnificaton ×320. (**b**) Etched in ammonium persulphate followed by dilute ferric chloride. In the centre of the photomicrograph the redeposited copper can be seen, with some grain detail in the form of lines of growth, set in the tin-bronze matrix of the dagger handle, showing cored grains and some areas of alpha + delta eutectoid. The redeposited copper is often twinned. Magnification x200

because of cooling slowly in ceramic moulds or the presence of substantial alloying elements such as arsenic or tin, which result in the solidification of higher-temperature phases first of all, and tin-rich or arsenic-rich liquid remains which then fills in the spaces between the dendritic crystals.

The silver-copper alloys, for example, are often heavily segregated, and the dendrites that begin to precipitate out may remain fixed in that state and composition when the alloy cools down to a solid state. The consequence of this is that the structure may be out of equilibrium and contain a series of dendrites surrounded either by the alpha (α_{Ag}) or beta phase (β_{Cu}) or the eutectic mixture itself. These kinds of structures, with dendrites or distorted dendrites as a result of working to shape, are quite common in ancient or historic silver-copper alloys. If alloys with low amounts of these alloying elements are annealed, then equi-axed grains can be produced as the dendritic segregation can be removed. If solute segregation has not been sufficiently removed by annealing before cold-working, banding occurs, which is shown in Fig. 4.15 for a tin bronze and in Figs. 4.16 and 4.17 for cupronickel-alloys with high amounts of iron and cobalt. This banding can persist across the recrystallized

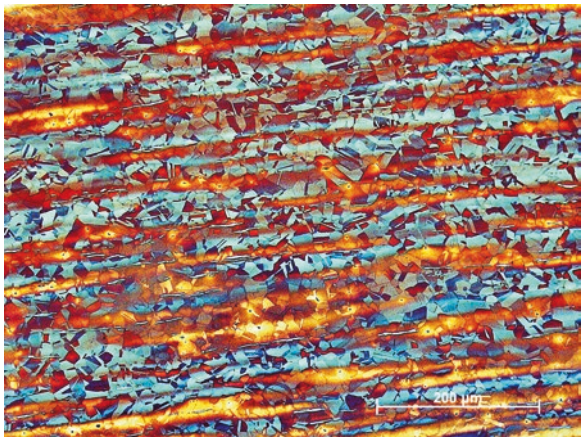

Fig. 4.15 Tin and antimony-rich banding in the microstructure, a late Bronze Age bronze ring with 3.6% of tin and 1.2% Sb from the Hünenburg, Germany. Etched with Klemm's reagent II

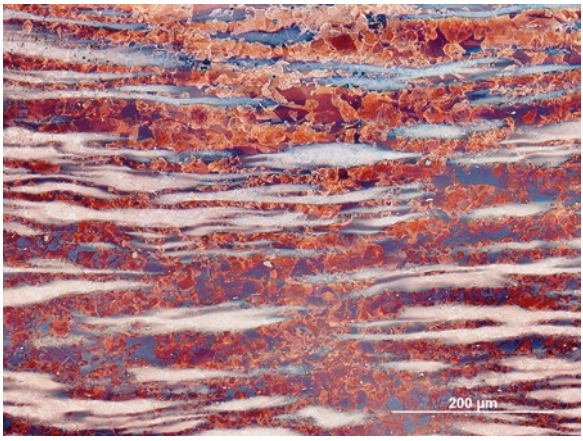

Fig. 4.16 Segregation of iron-nickel-cobalt-rich phases within the microstructure of a high-nickel copper alloy of a pin from Kesikkaya, Turkey. The recrystallized non-segregated grains of the copper-rich phases are revealed by Klemm's reagent III, whereas the segregations were not attacked by the etchant. The alloy contains 22% nickel, 5.8% iron and 2.7% cobalt and has a mean hardness of 180 HV 0.1 ± 10

grains and can be seen as shadows or lines on etching the sections of the objects under examination.

Banding of residual dendrites is very often observed in arsenical copper alloys, as shown in Fig. 4.18 [14, 55, 88], while banding in silver alloys can also be due to residual dendrites but is mostly influenced by the micro-segregation of solute elements due to cold-working [46, 54, 55, 124].

Highly leaded alloys were quite popular in the European Iron Age and Hellenistic and Roman period, as well as in Asia. Some examples of these types of alloys include Chinese bronze mirrors, whose classical composition calls for 25% tin, 5%

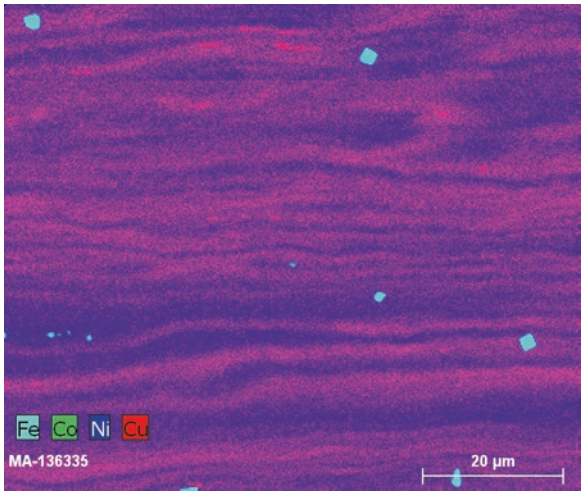

Fig. 4.17 Qualitative pseudo-coloured EDX-dot map of a wire ring from Boğazköy, Turkey. The alloy contains 20.7% nickel and 1.2% cobalt

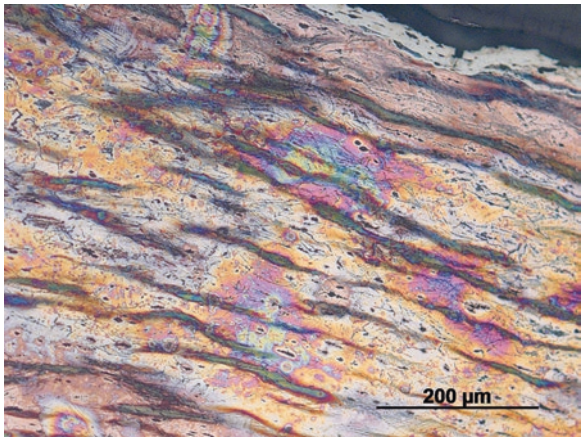

Fig. 4.18 Arsenic segregation of residual dendrites and silver-coloured cubic γ-phase ($Cu_{3-x}As$) on the surface of an eneolithic dagger from the cemetery of Singen, Germany. The alloy has a mean content of 5.2% arsenic; the γ-phase shows 27.5 to 29% arsenic

lead and 70% copper. Roman bronze mirrors, with less tin and more lead, up to about 8% lead were made in the Roman Iron Age.

An example of a heavily leaded bronze microstructure is shown in Fig. 4.19, a bronze Herm, in the collections of the J. Paul Getty Museum. The lead has pooled to some extent in certain areas of the heavily leaded casting. Segregation is quite common in these alloys. It is unusual for the lead to sink down through the alloy, in many cases it remains inside the alloy and in German is known as "Blocksaigerung" as the lead-rich phases follow the heat and agglomerate at the hottest spots, which is usually internal to the artefact concerned.

The casting condition is one of the most important factors involved in this phenomenon (see Hanson and Pell-Walpole [34]), but mould material, gating systems and the presence of elements such as tin, arsenic and antimony have a significant

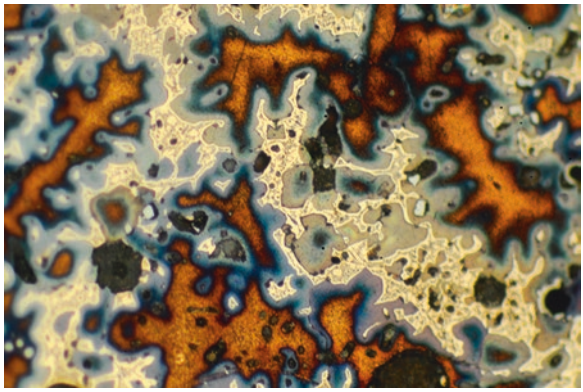

Fig. 4.19 Microstructure of a Greek bronze Herm in the collections of the J. Paul Getty Museum. The cast bronze Herm, a leaded bronze with about 8% tin content, 5% lead, is in the cast condition, with prominent coring present and areas where the alpha + delta phase of the bronze system can clearly be seen. Etched in ferric chloride, magnification ×120

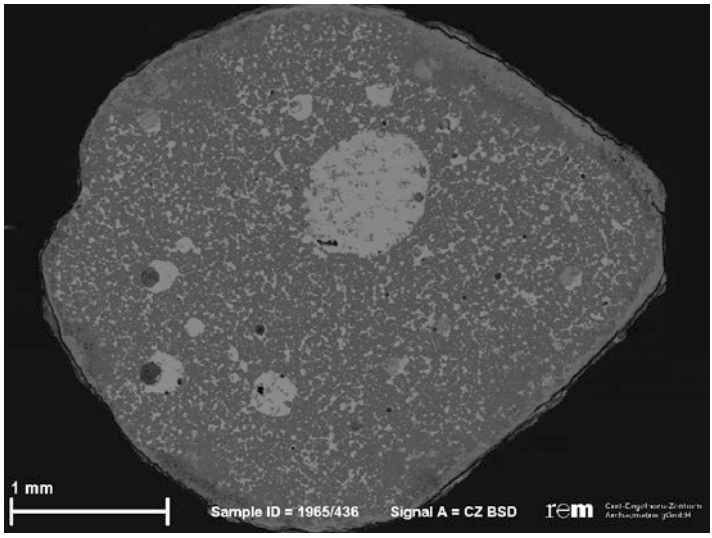

Fig. 4.20 SEM-backscattered electron image of a Late Iron Age ring from the oppidum of Manching, Germany with a mean lead content of 26% and 6.5% antimony shows heavy lead segregation in the centre and a mean hardness of 80 HV 1

negative effect on the segregation properties of copper-lead alloys. Figure 4.20 is a cross section of a typical Late Iron Age ring with a mean lead content of 26% and 6.5% antimony. The microstructure consists of randomly distributed lead particles and some macro-segregated drops of coalesced lead containing dendrites of α_{Cu}-solid solution, $\delta_{(Cu\text{-}Sb)}$-phase ($Cu_{4.5}Sb$) and globular sulphide (Cu_2S). The segregation of the lead has caused a monotectic reaction, when copper-rich α_{Cu}-phase, the $\delta_{(Cu\text{-}Sb)}$-phase and cooper sulphide decomposed from the liquid with decreasing temperature.

4.4 Pores and Non-metallic Inclusions

4.4.1 Pores

As mentioned above, the microstructure of an object consists not only of its metallic compounds but also of compounds of metals and non-metals, of non-metallic constituents and finally of pores. Porosity is commonly observed in ancient metals and often produces difficulties in castings. Casting defects and shrinkage cavities frequently occur within large castings, such as life-sized statues. Figure 4.21 shows a typical dendritic appearance of pores.

These occur when the casting system is not available to compensate for shrinkage during the transition from the liquid to the solid state. The so-called solidification contraction is due to the fact that solid metals have higher densities compared to the liquid and the molten metals decrease in volume as they solidify. When the alloy solidifies non-uniformly because of variations in temperature due to different wall thicknesses, inappropriate gating systems or other problems, local volume deficits can form cavities. Shrinkage cavities can contain gases or segregated metallic compounds such as lead or eutectic components. Gases such as oxygen or hydrogen are always present during the production of metals, and gas-metal reactions can form a variety of undesirable effects. Blowholes are casting defects that result in the evolution of gas bubbles entrapped in the solidifying metals (see Chap. 3, Fig. 3.20). Actually, most of the gas rises to the surface during solidification and escapes by spitting the hot liquid metal around. Pliny ([83], 34, 96) refers to this negative effect of hydrogen in the casting of large statues, which is due to the increased air moisture during summer time: *"Id quoque notasse ab re est, aes omne frigore magno melius fundi." (It is also not out of place to notice that all copper and bronze fuses better in very cold weather).*

Fig. 4.21 Heavy cored bronze casting waste from the oppidum of Manching, Germany with dendritic appearance of pores. Unetched specimen containing 9.5% tin and 7.2% lead

4.4.2 Non-metallic Inclusions

Blowholes and spitting are not the only effects of gas-metal reactions. These can form non-metallic constituents. There are usually extensive miscibility gaps in the liquid state and complete immiscibility in the solid state between metallic and non-metallic phases, such as oxides, silicates or sulphides. Therefore some non-metallic constituents exist already as separated liquid phases or as solid particles in the molten metal, or others are soluble in the melt and become distinct precipitations when solidification occurs. In any case, non-metallic phases are coarsely or finely dispersed in the solid metal as distinct inclusions. The inclusions in ancient metals are a valuable source of information as non-metallic inclusions cannot recrystallize during cycles of working and annealing and so act as additional messengers of change from the cast to the worked state. As working proceeds, inclusions tend to become flattened and elongated along the length of the section, and they retain this characteristic throughout their material existence, as illustrated in Fig. 4.22.

In heavily corroded alloys, where the bulk of the metal has been totally lost to corrosion, non-metallic inclusions can provide important clues as to whether the object has been deformed by working and annealing or is in a cast condition. This is because the inclusions are preserved in the corrosion products and, if elongated along the length of the section, are an indication that working and annealing, or hot-working to shape, has occurred.

There are different sources and reasons for non-metallic inclusions. Especially in pre-industrial metallurgy, there are a large variety of different non-metallic constituents. Modern metallurgy considers such inclusions to have deleterious effects on metals and should be eliminated if possible. Inclusion rating characterizes them by origin, and so they are classified to generally fall into two groups, those of indigenous and those of exogenous origin [122]. Indigenous inclusions can occur because of the reaction of the hot or molten metals with gas, when metals become compounds by oxidizing during manufacturing processes or due to their limited solubil-

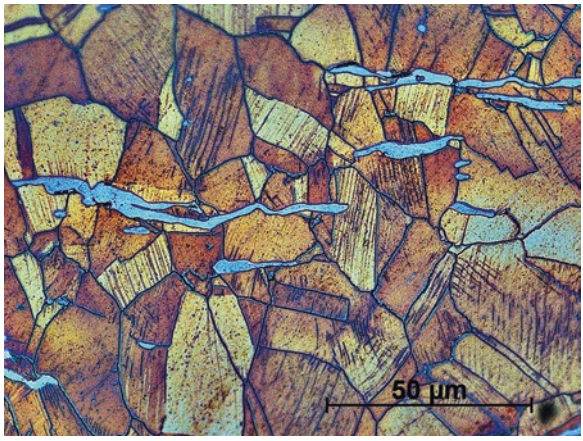

Fig. 4.22 Elongated copper sulphide ($Cu_{2-x}Fe_xS$) inclusions within the annealed and cold worked microstructure of Early Bronze Age miners pick from the Mitterberg mining district, Austria with a maximum hardness of 350 HV 0.1. Volume fractions of the inclusions have been determined to be 3.9–4.8%

ity in the solid metals. Exogenous inclusions form by interaction of molten metals with non-metallic material such as slag, furnace linings, moulds or crucibles. This classification is helpful, but cannot be transferred one-to-one to non-metallic inclusions of ancient metals. Most of the inclusions in ancient metals would be classified as those of indigenous origin, even when they are constituted with the involvement of exogenous sources. Similar to modern metallurgy, non-metallic inclusions are best known from ferrous alloys but especially as a result of the bloomery process (Chap. 5), where they derive from different origins than those in modern steelmaking processes. Due to the solid-state reduction of iron ore to solid metal, all wrought iron produced in the bloomery process usually contains large volume fractions of slag inclusions, which originate from the first step of production, the smelting process. Iron can already be reduced from its oxides at about 640 °C, which is considerably below the melting point of iron at 1535 °C [59]. However, the iron ores contain numerous impurities such as silica or alumina, often referred to as the "gangue" minerals, which must be removed if the smelting is to be successful. To achieve this, these minerals must be separated out as a liquid slag, for which the temperature in the furnace must be kept at about 1150–1350 °C, and it is this which can be difficult to achieve while also retaining enough carbon monoxide to effect reduction of iron [81, pp. 131–140]).

To separate metal from slag, the slag should be of low viscosity to create a liquid or pasty mass or retain enough fluidity to be tapped. The viscosity of slag depends on the basicity of the slag, as alkaline oxides lower the viscosity of slag significantly [1], for which reason fluxes such as limestone could be added. Actually, there is hardly any evidence for deliberate flux additions to European bloomery processes before medieval times, when the earliest blast furnaces in Europe were developed [11, 12, 81]. Therefore, metal-slag separation usually has not been very effective, and most bloomery iron contains large volume fractions of slag inclusions, which predominantly derive from the smelting and contain information about the process and the ore used. This information can be retrieved utilizing analytical methodologies with a high-spatial resolution. Electron microanalysis is capable of revealing the smelting conditions, but for information concerning provenance of the iron, more sensitive methods such as laser ablation-inductively coupled plasma-mass spectrometry (LA-ICP-MS) should be used (see Coustures et al. [19]; Dillmann et al. [27]).

In contrast to modern steel, the inclusions in early bloomery iron are exclusively oxides, with iron oxide, wüstite (FeO) and iron silicate and fayalite (Fe_2SiO_4) as the main phases, shown in Figs. 4.23 and 4.24, whereas higher iron oxides do not survive the reducing conditions necessary to produce metallic iron but are present within purifying slag of later periods [11, 12]. The iron oxide phases are usually embedded in a matrix of glassy components with decomposition of silicate or spinel group minerals such as leucite or hercynite [11]. There is a correlation between the metal structure and certain mineral phase assemblages within the inclusions, which has already been described by Buchwald and Wivel [13]. Depending on the ratio of carbon monoxide (CO) and carbon dioxide (CO_2), the microstructure of bloomery iron can be very varied.

Fig. 4.23 SEM-backscattered electron image of a slag inclusion with wüstite dendrites in fayalite matrix within the ferritic part of a bloom from a shipwreck discovered close to Kyrenia in Cyprus and dated to the fourth century BC. Mean volume fractions V_V of the inclusions have been determined to be 11% ± 5

Fig. 4.24 SEM-backscattered electron image of fayalite and glass components of a slag inclusion within the microstructure of a Mongolian belt buckle from a rock tomb of Nükhen Khad in the Zhargalant Khairkhan mountains, dated to the sixth to eighth centuries AD

Figures 4.23 and 4.24 show typical iron-rich slag from ferritic or ferritic-pearlitic microstructures, whereas Fig. 4.25 shows glassy slag within pearlite. The volume fractions of wüstite, fayalite and glassy components correlate with volume fractions of ferrite and pearlite, because of the decomposition of wüstite to iron and the carburization of the iron within a reducing atmosphere (see Buchwald [11]; Buchwald and Wivel [13]).

Wrought iron does not only contain inclusions which originate from the smelting process. Every forging must be done under red heat, and this leads to oxidation of

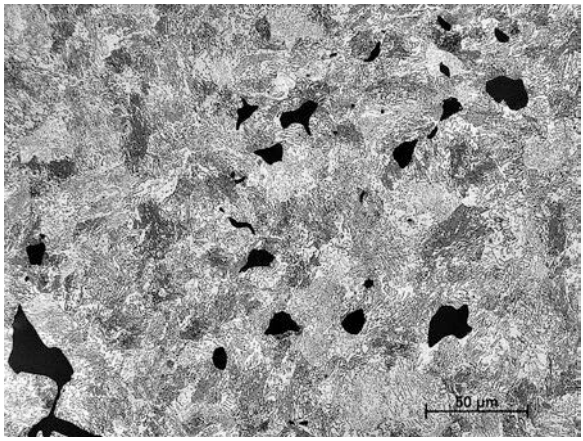

Fig. 4.25 Glassy slag inclusions within the pearlite-rich part of the iron rack of the bronze couch from the Hochdorf tomb, Germany, which is dated to the Early Iron Age (Ha D). Etched with nital

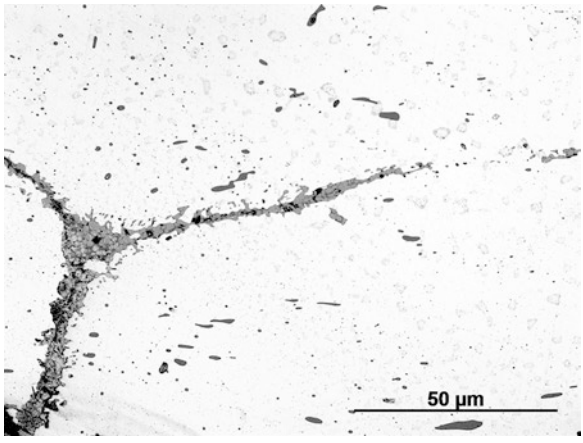

Fig. 4.26 Wüstite slag inclusions along the welding seams of a pattern welded early medieval sword

some of the iron. The fabrication of composites had to be carried out by forge welding (Chap. 5), and the need for fluxes for this process introduces new slag components. Figure 4.26 shows a massive formation of wüstite in the weld seam of an early medieval pattern welded sword from Mannheim, Germany.

With the rise of the indirect process following the development of the blast furnace during the Middle Ages, the characteristics of non-metallic inclusions in iron and steel change drastically. As with industrial steels, most inclusions derive from the fining of the cast iron, and most elements in the inclusions are oxidized minor constituents reacting with exogenous impurities [26, 50]. Iron sulphide inclusions (FeS_2) have been found in a pig iron from a high medieval smelting site near Reutlingen, Southern Germany, shown in Fig. 4.27. It is quite unlikely that the ironworkers were already using coal, but some ferruginous sandstone deposits are chatted with pyrite, which might have been used.

In copper alloys, sulphide inclusions tend to be more prominent constituents than oxides, but there are also a variety of compounds and minor accompanying ele-

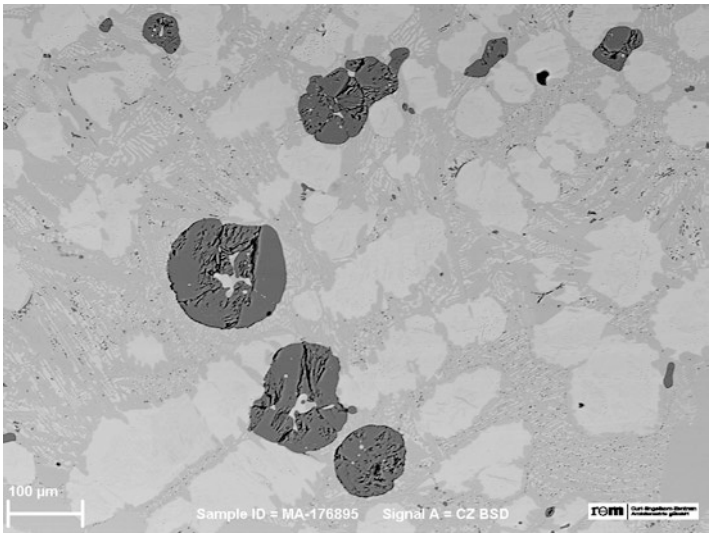

Fig. 4.27 SEM-backscattered electron image of iron sulphide (FeS_2) inclusions of a metal working debris from a smelting site near Reutlingen, Germany. The hypo-eutectic microstructure of the metallic matrix is already visible in the unetched state

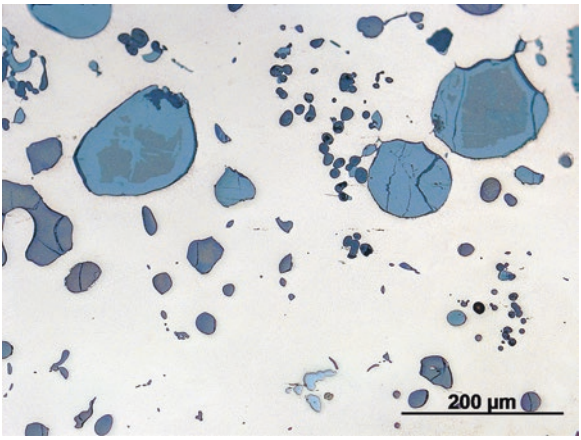

Fig. 4.28 Matte inclusion (dark-grey) and partly converted matte inclusion (blue-grey) in a planoconvex ingot of black copper from Urnfield period ingot storage. Metallic iron is light grey. Unetched and in bright-field illumination

ments within these inclusions. The determination of the bulk compositions of copper alloys is biased since some of the elements detected are present as components of the non-metallic inclusions, as well as metallic phases. Figure 4.28 shows a cross section of a late Bronze Age planoconvex raw copper ingot from Burladingen in Southern Germany. The mean volume fraction of the sulphide inclusions has been determined to be 8% (±2.2) by area analysis. Most of these inclusions contain iron in variable amounts. Contrary to the statements of Craddock [21], there is ample evidence for a matte smelting process in the Eastern Alpine region during the Bronze

Age (see contributions in Stöllner and Oeggl [117]), and according to this practice, most of the inclusions of that ingot are stoichiometrically related to the matte mineral bornite (Cu_5FeS_4). Indeed part of the iron is already removed by roasting, so that there are also iron-bearing copper sulphides ($Cu_{2-x}Fe_xS$) and some pure copper sulphide inclusions (Cu_2S) present, as seen in Fig. 4.22.

The total iron content of the sample has been determined by XRF to be 2.8%, which represents not only all the copper-iron-sulphides but also the metallic iron, which is precipitated from the molten copper (see Sect. 5.2). Matte inclusions rarely survive refining, alloying and casting of copper unchanged, but many sulphide inclusions of ancient copper alloys still contain iron ($Cu_{2-x}Fe_xS$), usually less than 1%. Sulphide inclusions of late Bronze Age cupronickel-alloys from Anatolia also contain nickel and cobalt [56], inclusions of paktong alloys (Chap. 5) contain nickel and zinc, while copper-arsenic-antimony alloys of the Nahal Mishmar hoard from the Judean Desert, dated to the fourth millennium BC, contain arsenic and antimony-bearing copper sulphide inclusions [119]. Sulphide inclusions may have traces of selenium and tellurium, which originate from sulphate-containing copper ores and which substitute part of the sulphur (see Rehren and Northover [91]; Zwicker [132]). The amount of selenium in copper sulphide inclusions is usually high enough to be established by EDX, whereas the concentration of tellurium is much less and its detection needs a more sensitive method of analysis such as WDS-EPMA.

In brasses, the iron content of copper sulphide inclusions is usually substituted by manganese (see, e.g. Barrena et al. [4]; Brüggler et al. [8]) and in paktong alloys as well. There are no investigations or experiments available to explain why this is the case at the moment, but the phenomenon is connected in all probability with the cementation process, when iron gets reduced and enters the solid solution (see Sect. 5.1). The compositions of non-metallic inclusions within brasses can vary within one object. Brasses usually contain copper-zinc or zinc-copper sulphides (CuZnS, $(Cu,Zn)_2S$, ZnCuS) or pure zinc sulphide (ZnS), rarely zinc-copper-disulphide inclusions ($ZnCuS_2$). They typically have traces of manganese and selenium. Zinc-bearing bronzes or gunmetal alloys do also show zinc-copper sulphides (see Willer et al. [129, Table 1]), but they still contain iron, because they derive from the bronze addition.

Copper oxide inclusions (Cu_2O) can derive from ores containing oxide or carbonate copper minerals or from the inner oxidation of copper. Native copper and raw coppers melted from sulphidic ores contain sulphide inclusions, but during melting it absorbs oxygen, and copper oxide inclusions can appear additionally to sulphides [125]. Eutectic and hypereutectic microstructures of copper and oxide are regularly found in casting waste (Fig. 4.7). Copper oxide inclusions in copper-arsenic alloys or copper-antimony alloys are often associated with other oxidized minor elements such as arsenic or antimony oxides [14, 73, 75], while more noble metals have no effects on the inclusions.

Other non-metallic inclusions in copper alloys, such as tin dioxide, cassiterite (SnO_2) shown in Fig. 4.29, are accidentally produced by the internal oxidation of bronze and rarely observed in artefacts (see Dungworth [29]), but they can be regularly observed in casting waste (Figs. 3.23 and 3.24). Scott [102], for example,

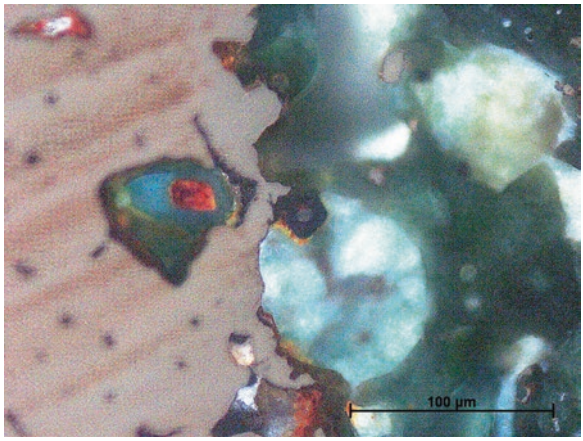

Fig. 4.29 Tin oxide inclusion (SnO_2) at the surface of fragment from a large Roman bronze relief from Mittelstrimmig, Germany, viewed under polarized light

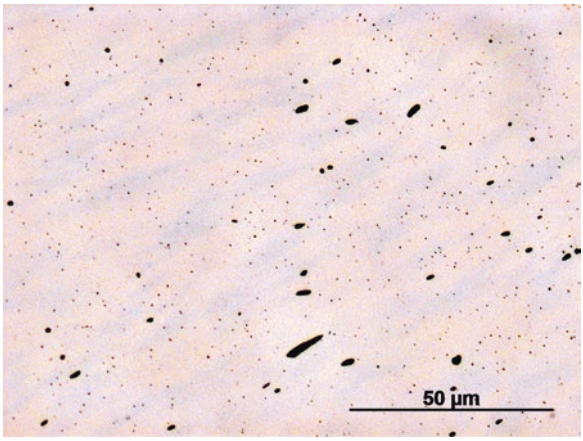

Fig. 4.30 Globular iron oxide inclusions (FeO) within the microstructure of a high-nickel (13.7% Ni) lunular pendant, from Boğazköy, Turkey. The mean value of iron determined by XRF is 2%, which is not only present in the oxide inclusions, but also in copper-nickel sulphide inclusions. The total volume fraction of the inclusions has been quantified to 0.4%. Imaged in bright-field reveal the segregations already in an unetched state

found small cubes or crystals of cassiterite in some Ecuadorian arsenical bronze alloys, which had been cast.

Iron and cobalt-bearing cupronickel-alloys from Anatolia show the presence of iron oxide inclusions (FeO), often containing variable amounts of nickel and copper shown in Fig. 4.30. They derive from the internal oxidation of the iron-bearing alloy [56]. Figure 4.31 shows iron oxide (FeO) inclusions within a Late Iron Age bronze scabbard from the Wederath cemetery in Germany. They are most probably of exogenous origin, although there is no reasonable explanation for their presence which can be stated categorically at present. Iron oxide inclusions in copper are rarely reported (e.g. Cope [18]), but some raw copper products, such as late Bronze Age

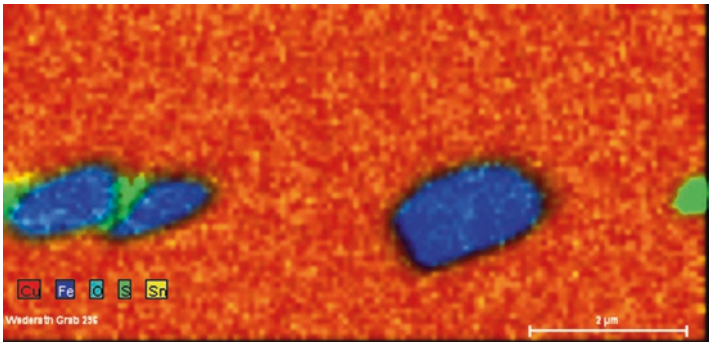

Fig. 4.31 Quantitative pseudo-coloured EDX-dot map of iron oxide inclusions within a Late Iron Age bronze scabbard from the necropolis of Wederath, Germany

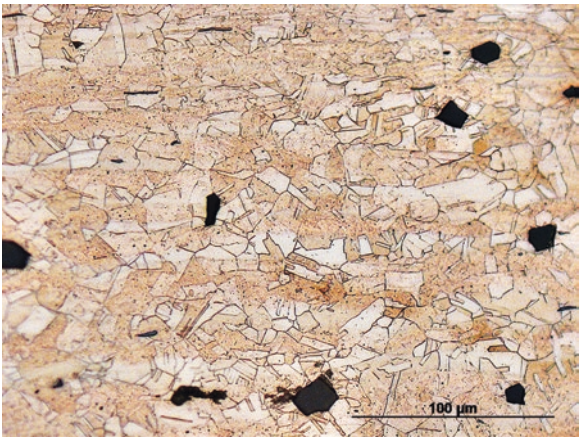

Fig. 4.32 Angular nickel-oxide inclusions (NiO) within a recrystallized matrix of a nickel-bearing α_{Cu}-solid solution of a needle from Boğazköy, Turkey. Etched with aqueous ammonium persulphate and viewed in bright-field illumination

oxide ingots or so-called *Aes rude* and *Ramo secco* bars from Italy, contain iron silicate slag and magnetite as relicts of the smelting process (e.g. Craddock and Meeks [22]; Ingo et al. [43]; Hauptmann et al. [37]; Matteoli and Storti [64]).

Nickel oxide inclusions, shown in Fig. 4.32, have been detected within a cupronickel-alloy from Anatolia [56].

The volume fractions of non-metallic inclusions in copper alloys can be several percent in raw copper and also in Early Bronze Age and chalcolithic items [49, 91, 118], but it is usually less than 1% in items of later periods (e.g. Willer et al. [129, Table 1]).

Silver alloys usually contain only copper oxide inclusions (Cu_2O), which derive from the inner oxidation of the silver alloy. An example is shown in Fig. 4.33.

Figure 4.34 shows a cross section of a silver disc fibula from the Early Medieval cemetery from Bedburg-Königshoven in the Rhineland, Germany. It contains a large volume fraction (11.5% ± 1) of tin dioxide inclusions (SnO_2), which are elongated along the length of the section. The mean tin content has been determined by

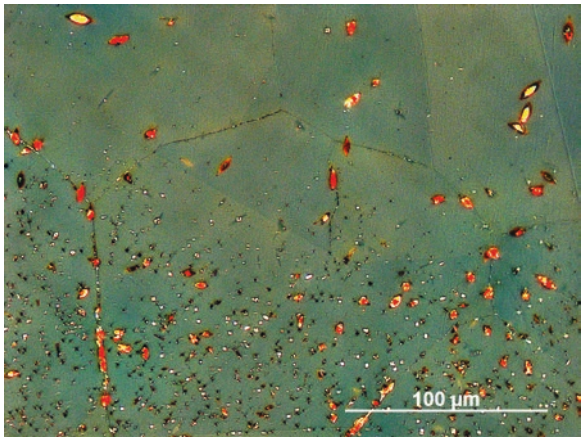

Fig. 4.33 Copper oxide inclusions (Cu_2O) near the surface of silver teeth of comb from Cumae, Italy, dated to the eighth century BC, viewed under polarized light after etching with potassium dichromate

Fig. 4.34 SEM/BSE image of SnO_2-rich inclusions in the microstructure of an early medieval silver disc fibula from the cemetery of Bedburg-Königshoven, Germany

XRF to be 8.9%. The maker of this fibula must have used scrap such as soft-soldered silver or bronze to produce the disc. By casting or annealing, the tin content of the alloy has been converted to oxides by internal oxidation, which caused fractures because of its hardness. Silver alloys are prone to this kind of oxidation as oxygen is quite soluble in hot silver. This can then oxidize the copper content to produce copper oxides.

Besides some copper oxide inclusions, which derive from internal oxidation, gold alloys are usually free of non-metallic inclusions. Indeed, X-ray diffraction studies have found both quartz and calcite inclusions in ancient Colombian gold

objects [45], both of which might be expected from the geological evidence. Gold objects from the ancient world can be flecked with platinoid inclusions, usually of the osmium-iridium group, as these are hard, cannot be molten and accompany the gold through its refining process [65]. Platinum-group metals are the common metallic inclusions in gold objects and, as these are not molten in the process of forming the gold object, behave very much like non-metallic inclusions. In some cases, the presence of these platinoid group inclusions is one line of evidence for the authenticity of the gold object concerned.

4.5 Plastic Deformation and Working and Annealing

Metals, when subjected to a force, can move to a certain, limited extent, by elastic deformation. This is termed as "recoverable" alteration, since when the force or load is taken away; the metal recovers to the same state that it was in before the force was applied. This kind of deformation is modelled by Hooke's law. In the elastic range, elastic modulus, so-called Young's modulus for the metal concerned can be determined. This can be plotted on a stress-strain curve, which is very important for the engineering properties of metals. Figures 4.35a and 4.35b shows the typical relationship between stress (force per unit area) and strain for a ductile metal such as copper. Young's modulus is given by stress/strain and has units of pressure. The yield strength is the region where deformation begins and strain hardening of the copper will then take place until the ultimate tensile strength is reached, when the copper starts to break apart until fracture occurs. Young's modulus for copper is 128 GPa, the yield strength about 322 GPa and ultimate tensile strength about 340 GPa.

Some metals, such as pure copper, may stretch elastically much more than hardened steel and will have a low value of Young's modulus as compared with the tough steel. In a stress-strain experiment, a cylindrical sample of the metal is pulled apart: it first stretches by elastic deformation and then by plastic deformation. The end of plastic deformation is characterized by a strain hardening region, and a necking of the test specimen occurs, which finally fractures and the metal then breaks, reaching the limit of its plastic deformation. In ductile fcc metals, such as copper, silver and gold, there is a large area of plastic deformation available. Steels can undergo plastic deformation too, but usually iron alloys have to be hot-worked in ancient usage, as they are too hard in the bcc state, as they can be worked in the high-temperature fcc region, making deformation much easier (Sect. 5.2). Metals can experience fatigue, which can occur in fcc metals, even in the elastic range of their treatment. This means that metallography is very important in assessing the formation of cracks in a variety of different alloying systems. In historic metalwork, for example, large outdoor sculptures made of zinc which were popular in many American and European cities, there is a severe danger of them fracturing, because the extent of plastic deformation of the metal is very limited. Therefore, elastic deformation occurs in these zinc sculptures, which either due to exceeding

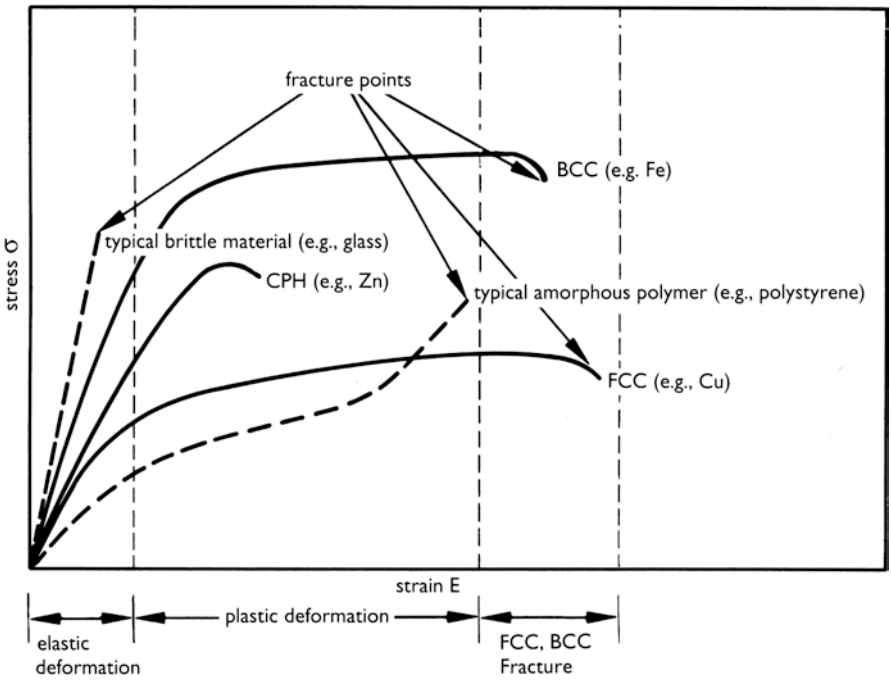

Fig. 4.35a Typical stress-strain curves for fcc, bcc and cph metals, compared with glass and a typical polymer. Fcc metals such as copper deform plastically for much longer than bcc metals such as iron. Cph metals such as zinc behave very differently than fcc metals like copper, because the cph lattice accommodates little movement by slip or dislocations compared with copper. In the elastic region, any elongation of the metal is recoverable if the applied stress is removed; the metal will return to its original shape. Once plastic deformation occurs, the shape is altered and cannot be returned to the original starting point

the elastic limit or metal fatigue over decades of exposure, they begin to break apart. Zinc is one of the metals of the cph system which tend to undergo mechanical twinning as they are deformed. This mechanism does not occur in fcc metals, such as copper, silver or gold.

Some ferrous alloys, in the bcc state, if heavily cold-worked can also show mechanical twinning. Metals, with very low plastic deformation, such as grey cast iron or white cast iron, are strong materials under compression but are very weak in tension. They are hard but brittle. This is why cast iron can be used as a support structure for historical buildings, where copper or bronze would be dangerous, as the latter are liable to too much plastic deformation. Cast iron is very hard but cannot undergo deformation by hammering. It cannot be used for making sword-blades but is good for absorbing the stress of compression.

The lattice of metallic systems is not perfect, and they have a number of dislocations of various types, particularly edge dislocations and screw dislocations. When a metal is plastically deformed, these dislocations pile up, until the metal becomes embrittled. These issues are discussed at much greater length in standard

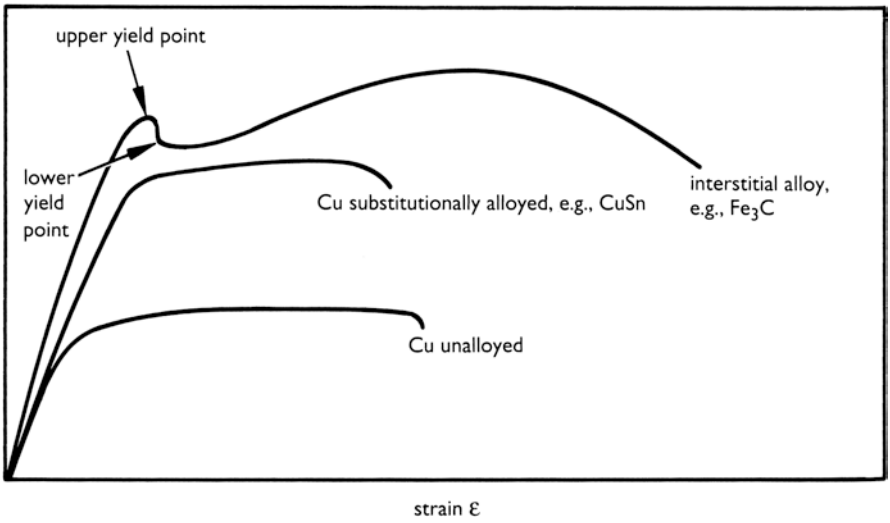

Fig. 4.35b Stress-strain curve for interstitial materials. Interstitial metals are small in size, such as carbon, and can be inserted into the lattice of some metals such as iron, to make steel. Interstitials tend to reside at the base of dislocations and anchor them. When slip occurs, carbon is left behind, and the dislocation is held until some higher stress is reached. When the stress factor is reached, an enormous number of dislocations occur that can now move at a lower stress than originally required; hence the two yield points for steels. Compare with the curve for unalloyed copper and for copper which is substitutionally alloyed with tin, as in the case of a bronze

metal textbooks (e.g. English et al. [30]; Hansen and Barlow [36]; Rodney and Bonneville [94]).

Annealing removes these congealed dislocations and returns the metal to a soft condition again. When fcc metals such as copper, silver and gold are worked and then annealed, they can recrystallize. The lowest energy system for this recrystallization is the formation of annealing twins. Annealing twins are mirror reflection planes of the atomic arrangement of the metal or alloy, and these can be revealed in a polished section by etching, when the rate of attack of the solid varies depending on the orientation of the metal crystals in three dimensions. When an fcc metal is cold-worked, the grains become distorted and elongated along the direction of working, and when annealed these grains will recrystallize to form twinned crystals with straight twin lines. An example from a Bronze Age bronze Palstave from Kent, England is shown in Fig. 4.36.

The other feature which may become apparent on deformation is that slip, or strain lines, may be evident in the crystal, because planes of atoms have slipped past each other due to heavy working. These strain lines are often unidirectional near the hammered surface of the object, or they cross over each other at certain orientations.

When the twinned and recrystallized grains are then further deformed, the crystals become distorted, and the twin lines become bent or curved. Further annealing

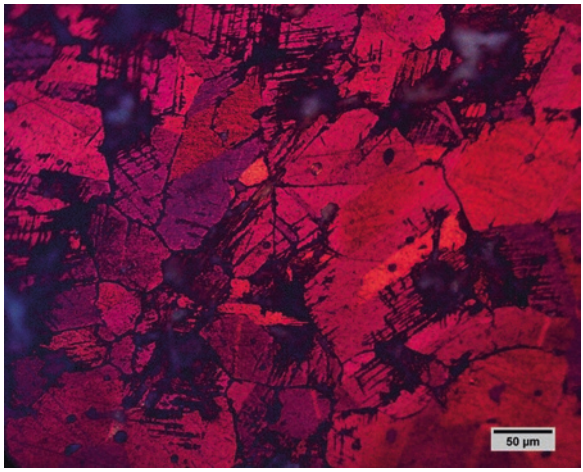

Fig. 4.36 Cold-worked cutting edge from a Late Bronze Age palstave from Kent with about 8.5% tin. Corrosion has outlined the strain lines through the grains seen here. Lightly etched in alcoholic ferric chloride

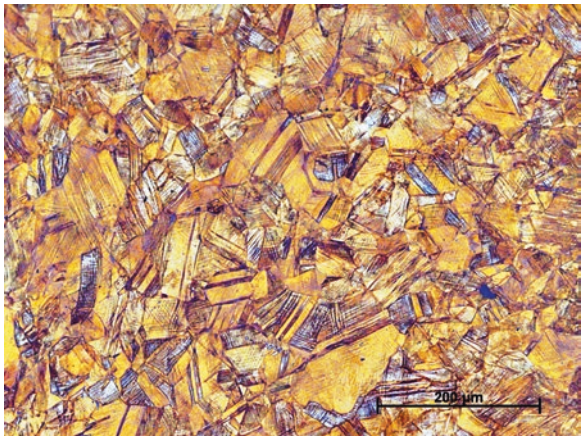

Fig. 4.37 Microstructure of a so-called Nauheim brooch from the Donnersberg oppidum, Germany shows heavy slipping and displaced twins. Etched with Klemm's reagent III

will reform the grains and create a new twinned grain structure, usually of a smaller size than those originally present. Some hot-worked alloys, such as struck coins, may retain a distorted grain structure.

Cycles of working and annealing are commonly used to shape copper and silver alloys. In order to avoid brittleness, the final working process is usually annealing. Chisels, knives, swords and palstaves may have their edges cold-worked in order to increase the hardness of the cutting edge, but also items like brooches were left worked to keep them semi-hard, as shown in Fig. 4.37.

Hot-working combines the effects of cold deformation and annealing in one stage and creates recrystallized grains. Not all alloys are suitable for being hot-worked, such as lead-bearing copper alloys, and some brasses are described as "hot-short". This phrase implies that the alloy concerned will tend to break apart on hot-working or become brittle.

Iron and steel alloys, which are bcc in their room temperature state, can only be slightly deformed by cold-working. The alloys must be heated to red heat by the blacksmith, in the austenite region of the phase diagram, in order to deform them successfully. As the iron alloy cools down, it reverts to the bcc state and must be reheated in the forge to successfully shape it. When body-centred cubic (bcc) metals such as iron are plastically deformed at normal temperatures, the type of motion that occurs depends on a number of factors, including the type and the rate of deformation. At low strain rates with moderate amounts of deformation, slip lines appear on the etched surfaces. Arrays of bands are known as Lüders lines or Lüders bands, which are caused by localized plastic deformation and usually occur in low-carbon steels after strain over the limit of elasticity. Lüders lines propagate at a front, which can move along the length of a tension with continued stressing. Slip lines in body-centred cubic metals are irregular and are usually described as "wavy" lines, which indicate that the dislocations are not confined to unique slip planes [71, p. 218].

Lüders bands are usually revealed by macro etching with Fry's Reagent [97, pp. 176–7]), which is not often suitable for small samples from archaeological objects. Figures 4.38 show the microstructure of a chain link from a Roman mail shirt. The chain links were die-cut from sheet metal, so that the grains around the hole are heavily deformed.

A different method has been applied to form Iron Age chain links from Bern-Tiefenau (Switzerland), which shows a textured microstructure in the longitudinal section in Fig. 4.39. The polycrystalline appearance of the grains and etching contrast is gone because they are axially aligned and elongated in the direction of principal strain. Such preferred orientated textures are best known from drawn wire, which is according to our present knowledge not yet known before the Viking Age (e.g. Odgen [77], 164), so that these chains would be the earliest examples, if their context would be secure.

Deformation twins, so-called Neumann bands, develop by extreme and rapid impact of stress. They were first described in iron meteorites but can occur in archaeological iron artefacts as a result of being heavily cold-worked. The twins

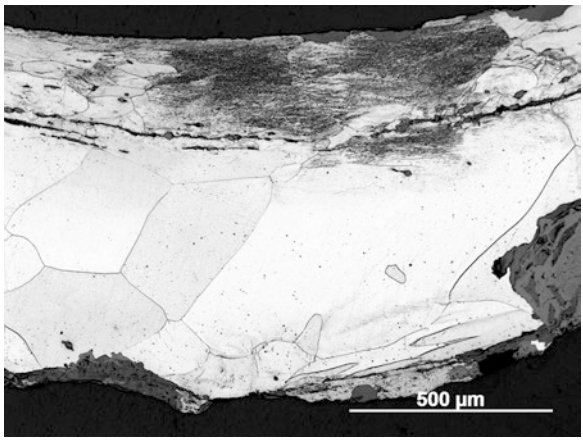

Fig. 4.38 Lüders lines at the inner side of a ferritic chain link from a Roman mail shirt from Lüttingen, Germany. Hardness values of such die-cut chain links varies from 150 to 250 HV 1. Etched with nital

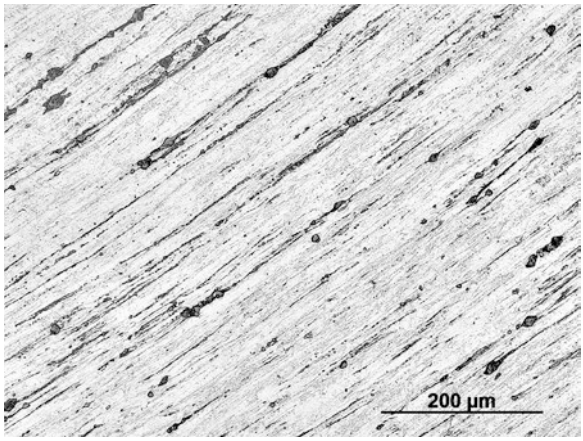

Fig. 4.39 Cracked slag stingers and unresolved microstructure of a ferritic chain link from an Iron Age mail shirt from Bern, Switzerland, having a mean hardness of 250 HV 1. Etched with nital

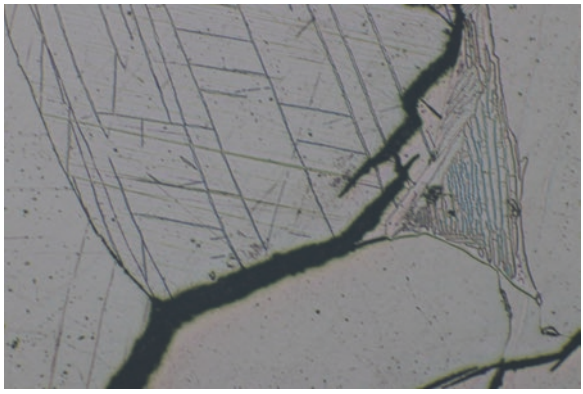

Fig. 4.40 Neumann bands in a heavily shocked meteorite from Chile. Magnification shown in scale bar, etched in nital.

usually initiate only in ferrite and never extend across a grain boundary. Neumann bands are regularly observed in the microstructure of ancient iron objects and are a clear indication for an impact shock (Fig. 4.40). Neumann bands often appear in ferritic hammers and European Iron Age swords [80, 100, p. 255]. The hammers clearly indicate the development of deformation twins during the use of the hammers as a striking tool, while the swords could have been occasionally cold worked [80, p. 152] or may have been destroyed during burial or devotional or religious ceremonies, as Uran [121, pp. 304–5] has pointed out. The Inuit, who used meteoritic iron quite a lot, practiced intentional cold-working to form and to sharpen their tools and weapons [10]. Knives of walrus ivory were made by inserting cold-hammered flakes of meteoric iron into a cut groove and holding them in place with bitumen or glue; small knives of caribou bone with meteoritic iron blades have been found from Inuarfigssuak, Greenland, originating from the Dorset or Thule culture [9, p. 411]). Examination of an ulo, or woman-knife, from Inuarfissuaq by Buchwald [9] showed a microstructure of distorted kamacite, with small sheared rhabdites and cloudy taenite lamellae, distorted from the cold-working which had been used to shape the iron.

Some brass and bronze alloys must also be hot-worked to deform them, such as high-tin bronzes with over 20% of tin. These alloys can be quenched, retaining the beta phase (Sect. 4.6.1.2), and this phase of the copper-tin system can be worked hot, around 700 °C, and then be shaped, before quenching, to retain the beta phase, followed by further working as required.

4.6 Solid-State Transformations

4.6.1 Non-diffusive Phase Transformations

4.6.1.1 Martensitic Transformations in Carbon Steels

Spontaneous diffusionless phase changes are generally termed martensitic transformations according to the best known and technically most significant transformations in the Fe-C system, but there are some nonferrous alloys where this kind of reaction is important as well. Martensitic transformations take place when cooling rates are fast enough to supress diffusion-controlled decomposition of high-temperature solid solutions and generally result in the formation of a distinct acicular microstructure called martensite, after the German scientist Adolf Martens.

The reaction ideally occurs by shear without changing the chemical composition, but in practice the cooling rates are not appropriate to transform all of the proportions of the solid solution into martensite (Sect. 4.6.1). The distinct acicular microstructure as a result of shearing is very characteristic for every martensitic structure and is readily recognized in the optical microscope after appropriate etching. This characteristic appearance of martensitic microstructures results from shape change of crystals due to their supersaturation of solvent atoms by those of the solutes. Ferrous martensite is principally a supersaturated solid solution of carbon in iron with a distorted form of α_{Fe} (bcc), which has become a body-centred tetragonal (bct) structure [51]. This transformation to martensite (bct) begins in the range from 400 to 200 °C depending on the carbon content. The interstitial solubility of carbon in unalloyed ferrite (α_{Fe}) is extremely low (0.02 wt %), whereas the high-temperature modification austenite (γ_{Fe}) is capable to solve between 0.8 and 2.11 wt % of carbon, independent of temperature, because of its larger interstices (see Sect. 5.3). Therefore the $\gamma_{Fe} \rightarrow \alpha_{Fe}$ transformation is accompanied by an atomic volume change and the decomposition of γ_{Fe}-solid solution into α_{Fe}-solid solution and carbon, which the latter is in fact not carbon but the interstitial solid solution cementite Fe_3C (see Chap. 5). Under equilibrium conditions, it would be a eutectoid reaction, where austenite decomposes into one of the most familiar eutectoid microstructures called pearlite: $\gamma_{Fe} \leftrightarrow \alpha_{Fe} + Fe_3C$. When iron-carbon alloys are heated above A_3 (see Sect. 5.2) and then plunged into water to quench austenite to room temperature, the carbon remains in solution, because there is not enough time to diffuse and to nucleate. But as mentioned before, the interstitial solubility of carbon in bcc α_{Fe} is extremely low, and additional interstitial solved carbon expands and

distorts the iron lattice, because regular positions are already occupied. Therefore, the transformation from γ_{Fe} (fcc) to α_{Fe} (bcc) is accompanied by shape deformation and volumetric expansion, which occurs according to the so-called Bain strain, uniformly expanded in two dimensions, but contracted in the third dimension and results in a tetragonal distorted crystal [3].

The initial surface of austenite is tilted and rotated by shear producing this very characteristic microstructure. Martensite can assume two types of morphologies. It crystallizes as acicular martensite needles if the carbon content is less than 0.6% called lath martensite, while above 0.6%, it assumes a plate-like morphology. These different morphologies are illustrated in Figs. 4.41 and 4.42.

Martensite plates grow very rapidly at speeds of the velocity of sound, which is why martensitic transformation is time-independent [3]. The change from austenite to martensite causes a considerable volume increase and different cooling rates between surface and core create additional stress, which can give rise to quench cracks. Iron Age files often show quenching cracks [100]. Compilations of the oldest quench-hardened iron objects of the Near East and Europe from the late Bronze Age to the Iron Age show that the possibilities of structural phase transformation of iron were recognized early on [53, pp. 200–201, 60, 82]) and some classic authors refer to the processing of iron in terms of heat treatments. Homer writes: *"…just as when a smith plunges into cold water a great axe-head or adze to treat it – for this is what gives strength to the iron – and it hisses fiercely, in the same way the Cyclops' eye sizzled around the olive stake…".*

TTT diagrams: The effects of the cooling rates on different iron and steel alloys can be followed using so-called time-temperature transformation diagrams (TTT diagrams), either isothermal or continuous cooling transformation diagrams (IT or CCT diagrams). The metallurgical literature often uses TTT as a synonym for isothermal transformation in general (see Krauss [51]). The isothermal TTT diagrams measure the rate of transformation at a constant temperature while time is varying. To derive an IT diagram, an iron alloy is heated to the austenitic region and then cooled rapidly to a lower temperature and held at that temperature, while the rate of

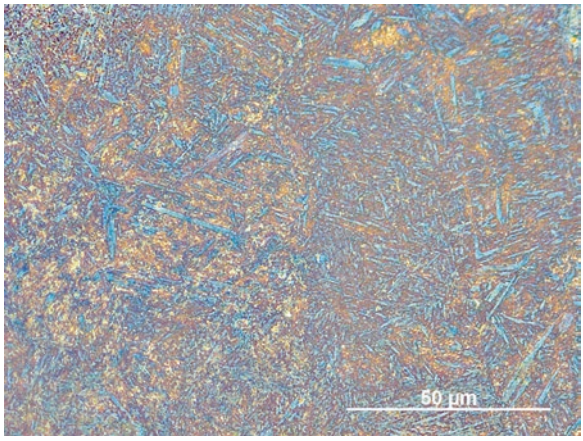

Fig. 4.41 Blue-coloured lath martensite in the microstructure of a Mongolian arrowhead from a rock tomb of Nükhen Khad in the Zhargalant Khairkhan mountains, dated to the sixth to eighth centuries AD. Maximum hardness of 660 HV 1 indicate a medium-carbon steel. Etched with sodium metabisulphite

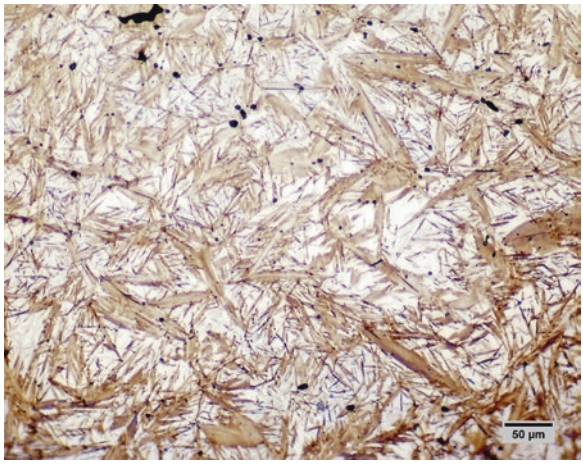

Fig. 4.42 Plate martensite in a cut French steel bead of the eighteenth century AD with a carbon content about 1.1% and a microhardness of 1000 HV. Made by cutting to shape followed by heating and quenching to create the martensite, followed by polishing like a gemstone to create the gem-like finish. Etched in picral

transformation is measured. IT diagrams are read along the time axes (Fig. 4.43). This kind of transformation never has been available to ancient blacksmiths, and the use of IT diagrams is very limited in its relevance to ancient ferrous alloys. More useful for ancient alloys are the CCT diagrams, as illustrated in Fig. 4.44, where the x-axis is the logarithm of time and y is temperature.

In the CCT diagrams, the extent of transformation as a function of time for a continuously decreasing temperature is measured. For example, an object heated to the austenitic region is cooled at a predetermined rate, and the degree of transformation is measured. CCT diagrams have to be read along the cooling curves.

4.6.1.2 Quenching of Copper Alloys

Microstructures analogous to the martensite of steel may be found in certain pre-industrial copper-tin and probably also in copper-antimony alloys. For low-tin bronzes, they may be quickly cooled which would affect the extent of dendritic growth, but the overall effects on the microstructure of the examples of bronze shown above would be slight. However, if the tin content is raised to more than 20%, then on quenching some of the higher temperature solid phases present in the phase diagram can be retained, producing an alloy with very different working properties than the cast equivalent. For alloys used as mirrors, the differences are not great in terms of working properties but become significant if the cast mirror is finished by turning on a lathe or if a cast bowl has to be cut and decorated after casting. Then the advantages of quenching these bronzes become apparent. Hot forged high-tin bronzes have been used in the Near East, in Central and especially Southeast Asia up from the mid first millennium BC to modern times for a variety of items (see Glover and Bennett [31]; Goodway and Conklin [32]; Northover [74]; Pryce et al. [84]; Ravich [87]; Srinivasan [111], Srinivasan and Glover [112].

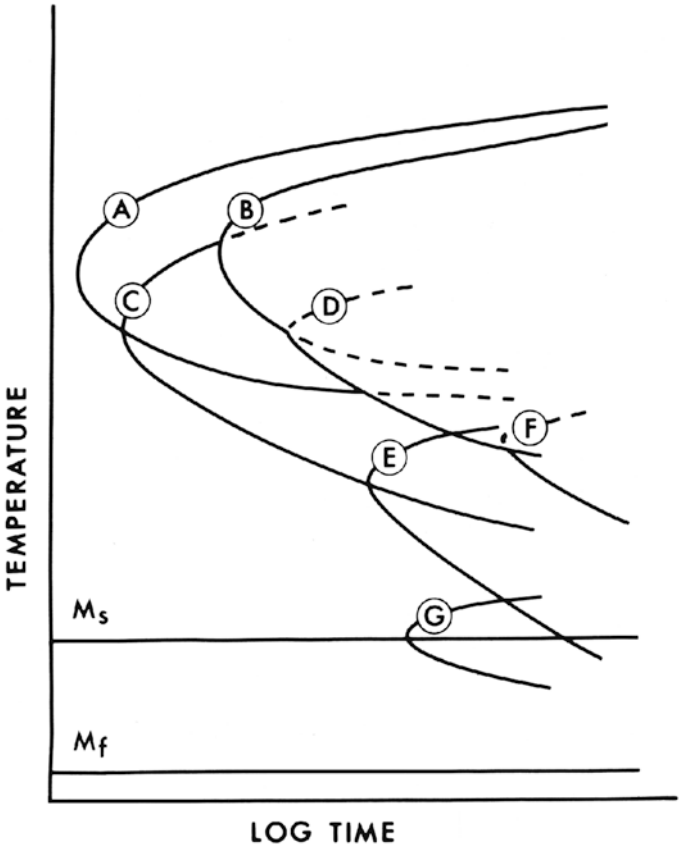

A: 0.01 vol fraction pearlite
B: 0.99 vol fraction pearlite
C: 0.01 vol fraction upper bainite
D: 0.99 vol fraction upper bainite
E: 0.01 vol fraction lower bainite
F: 0.99 vol fraction lower bainite
G: 0.01 vol fraction martensite

Fig. 4.43 Schematic IT diagram for plain carbon eutectoid steel (after Samuels [97]). For transformation according to IT diagrams, the specimens are cooled rapidly to IT temperature and hold there for a specific time and then quenched to room temperature

An example of the microscopic effects of quenching is shown in Fig. 4.45, part of a high-tin bronze bowl from the site of Ban Don Ta Phet, Southwest Thailand, dated to about 100 AD, of composition 22.7% tin and 76.2% copper.

Excavations on behalf of the Thai Fine Arts Department revealed a series of inhumation burials with 163 bronze vessels, 38 bronze bracelets, 7 bronze anklets, 16 bronze rings, 1 bronze ladle, 3 bird finials, 3 bells, and 579 iron artefacts and other material. The metalwork from this site has been published in summary form by Rajpitak and Seeley [85]. Etched beads suggest a date in third to second century BC. The bronze bowls ranging from 5 to 15 cm in diameter [85] are very thin, with

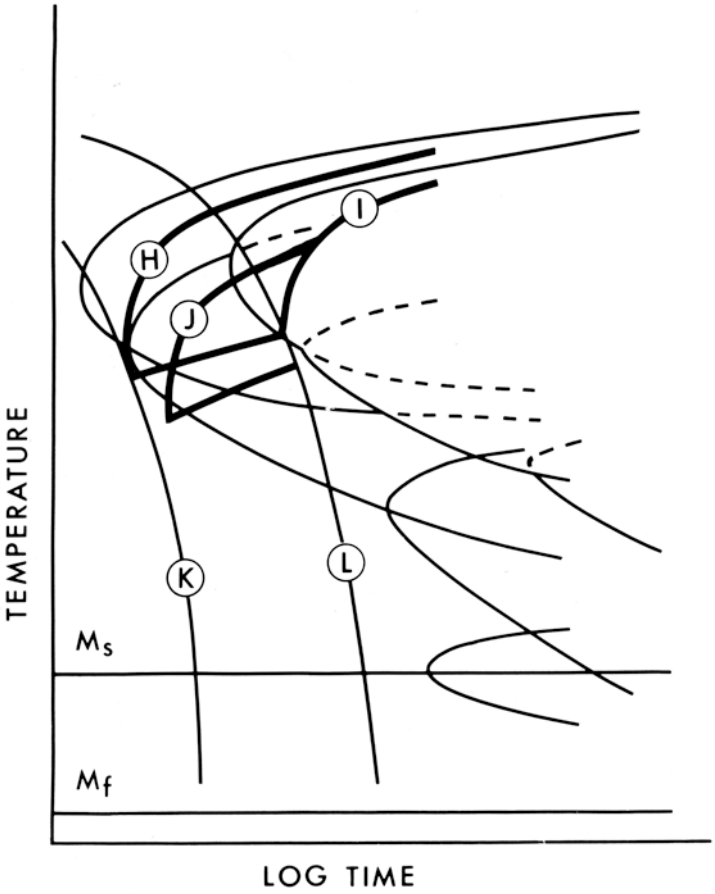

H: Start of transformation to pearlite
I: Finish of transformation to pearlite
J: Start of transformation to upper bainite
K: Critical cooling rate for suppression of diffusional transformation
L: Critical cooling rate for complete diffusional transformation

Fig. 4.44 Schematic CCT diagram for plain carbon steel (after Samuels [97]). Critical cooling rates K and L indicate complete non-diffusive and complete diffusive transformation of austenite. M_s marks the start of a martensitic transformation, while M_f is the temperature at which it is essentially complete. The curve H indicate the pearlite formation and curve J the bainite start. (After Samuels [97] Fig. C11 Courtesy American Society of Metals)

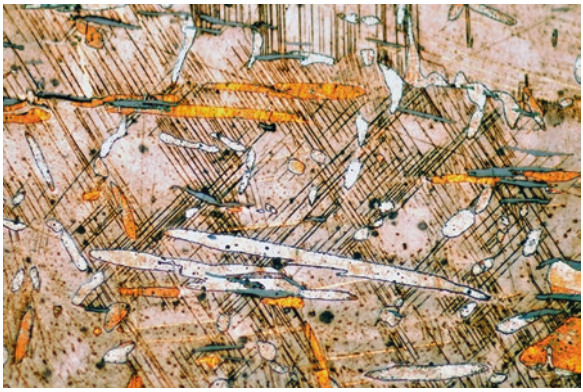

Fig. 4.45 Thai bronze bowl from the site of Ban Don Ta Phet, showing twinned alpha grains in a beta matrix. These twinned grains arise from the casting, heat treatment, quenching from about 650 °C, then reheating, hot-working, and subsequent quenching of the 22.7% tin bronze alloy, resulting in a beta or beta and gamma phase matrix with twinned alpha phase islands. Colour etched in Klemm's reagent II, magnification 280×

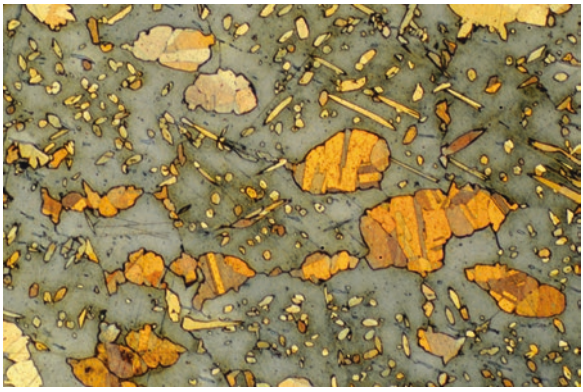

Fig. 4.46 High-tin bronze bowl, about 21.5% tin from Ban Don Ta Phet, quenched beta bronze, showing some alpha islands with the acicular beta-phase needles in the matrix of the cast, reheated and quenched bronze. Quenched from about 650° C. Colour etched, magnification ×280. Note that the twinned grains show straight twin lines as a result of hot-working to shape, where the hot-working combines deformation and recrystallization

wall thickness of 0.3–0.5 mm and with fine incised decoration. These bowls are made in a quenched high-tin bronze, such as that revealed by the section shown in Fig. 4.46. The 21–23% tin bronzes require heating to at least 300 °C before they can be worked [16], and the microstructure shows that it has been quenched from above 520 °C, which as we have already discussed is in the beta-phase field [89, 90]. Comparable fragments of high-tin bronzes have been reported by Marshall [62, 68] from Taxila, the ancient Gandharan capital on the North West Frontier of India, mostly from late phases, but Bhir Mound, the Mauryan city, from third to second

century BC contained a pair of bowls one with 21.55% tin, the ideal composition, as the microstructures shown in Fig. 4.46 are typical and show a preference for some alpha phase together with beta, rather than with slightly higher tin contents which are all beta phase.

This shows that the composition of these special alloys was very carefully controlled. Other important mentions of these alloys are those of Smith [109] from Pimai; Phase III at Ban Chiang [128], dating to 500–0 BC, a bronze bowl from Coimbatore, South India, and artefacts from Adichanallur in the Nilgiri Hills [7], two Koryu Dynasty bowls from Korea [123] and some Islamic bronze vessels from Iran [70, 74]. Rajpitak and Seeley [85] mention the account of Nearchus in his description of India written in the fourth century BC, fragments of which survive in Strabo's geography (Strabo 15.1.67) which states that Indians used vessels which were cast rather than beaten and which broke like pottery when dropped on the ground. This suggests that the brittle high-tin bronzes may well be described here. Recent work in South Indian by Srinivasan [111] and Srinivasan and Glover [112] confirms the evidence for use in this area, as the bronzes are still being made by traditional methods. Metallurgical investigations on bowls and vessels from Nilgiri megaliths and Adichanallur burials showed they consisted of 23–25% tin wrought to between 0.2 and 1 mm with a Vickers Hardness of 290–300 HV.

A bowl excavated from Taxila dated to 1000 BC showed it to be a beta bronze with 24% tin. Three samples excavated from Mohenjo-daro thought to be dated to 2500 BC were found to contain 22.1% tin, 22.2% tin with 14% lead and 26.8% tin. Srinivasan and Glover [113] found that yet another extant tradition of mirror making in South India utilizes cast alloys with 32% of tin, retaining a cellular delta microstructure such as that shown in Fig. 4.47, where Neville and Haycock show the same kind of structure, namely, delta phase in a matrix of alpha + delta, for their 31.2% tin bronze.

Srinivasan and Glover [113] provide an account of the casting of mirrors in the village of Aranmula, Kerala. These are very close to the composition of the delta phase, $Cu_{41}Sn_{11}$, whose ideal formula is 32.55% tin. The technique involves the use of a special closed crucible with attached mould, the account of which is of some

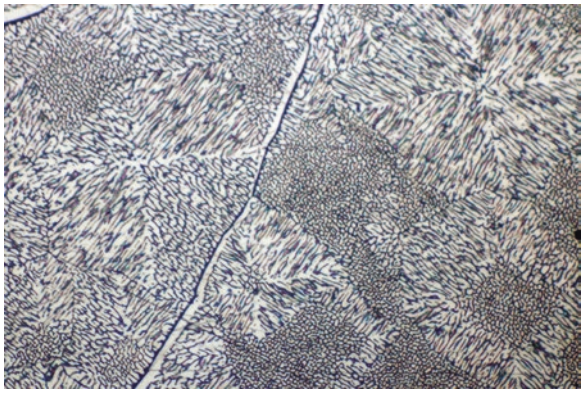

Fig. 4.47 Cellular delta microstructure from the cast condition of bronze with 28% tin

interest. The hardness of the delta phase when cast is extraordinary, reaching values of 500 HV, harder than that of a medium-carbon steel, which is around 400 HV.

There may be a number of reasons for this choice of alloy. Firstly, the high-tin alloys are not injurious to health for food-keeping as a brass bowl would be; secondly, the quenched alloy can be hot-worked to shape it and can be ground or cut to decorate the surface in a way in which the high-tin alloys cannot if slow-cooled because of the brittle delta; and thirdly for the colour. The 23% tin bronze is a good golden colour that could be visually attractive and simulate gold. The alloy, while not too brittle, is hard, with Vickers numbers between 180 HV to 260 HV.

As the alpha phase in these alloys is frequently twinned, we can reconstruct the fabrication methodology from the microstructure. Firstly the alloy is carefully made of exactly the right composition and cast into shape, roughly, probably in a mould. Then the alloy is reheated above 600 °C and hot-worked. The alloy is reheated above 600 °C and quenched. It undergoes a martensitic transformation to the beta phase.

The alloy can now be turned on a lathe to smooth the surface or to cut decoration into the surface of the bronze. It can be reshaped if necessary by reheating again, working and quenching, followed by polishing to finish.

We know that operations such as this must have been involved, for otherwise the alpha phase would not be twinned from the hot-working process as Fig. 4.46 reveals. Examination of the etched section shows the presence of some alpha phase copper-rich grains, sometimes acicular and which occur in areas with specific orientation as well as a random scatter. The overall cast structure of these types of high-tin alloys can be seen in Fig. 4.48.

In the background matrix of this bronze is a banded martensite, a variety of the β phase that proves that the bowl must have been quenched from the temperature region of 520–586 °C. This is slightly lower than the usual quenching temperature for these bronzes, which is generally in the 650–750 °C range. Some additional studies of the composition of these alloys confirm the general impression that the metalsmiths were deliberately striving for a composition which includes the alpha and beta phases, without knowledge, of course, of the phase relationships, but

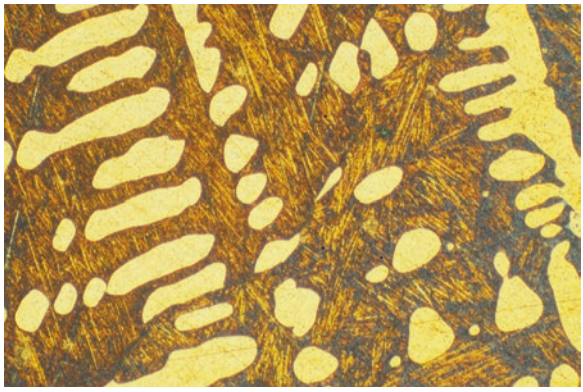

Fig. 4.48 High-tin bronze alloy in cast and quenched condition showing the suppression of the delta phase in the background, where beta-phase needles occur and with prominent alpha-phase dendritic cast structure. Etched in ferric chloride, magnification ×120. From the site of Ban Don Ta Phet, Thailand

purely from their sophisticated observations on the behaviour of metals. A study by Park and co-workers [78] showed that, on deformation, the small amounts of alpha present in the 22% tin bronzes, spanning the grain boundaries, act as micro-bridges interlocking the adjacent grains. The alpha phase apparently reinforces the boundary regions, an effect which is very sensitive to the alpha fraction and can be best obtained with tin contents close to 22%.

The hardness data obtained by Rockwell hardness testing is between 99.5 and 105.5 HRB for a 22% tin bronze [78]. Bowls from Korea, from the Unified Silla period (668–935 AD) made in this alloy, have wall thicknesses of 0.2 mm. Even a minor change in tin content, to 24% where the microstructure is entirely beta, would not have allowed this degree of hot-working. Here the phase diagram and its application is an essential component to understanding the microstructure of these quenched alloys. When quenched from high temperatures, the β phase is retained, and the alloy undergoes a martensitic transformation.

Time-temperature transformation or continuous cooling transformation diagrams are important in understanding the nature of the changes which may take place on cooling alloys at certain defined rates, as already mentioned above. The chart shown in Fig. 4.49 is the work of Goodway and Conklin [32] and shows that if very fast cooling takes place in the log time axis closest to the origin, then the whole structure will be martensitic. Less drastic cooling conditions will create a range of different options in which the start of the martensitic transformation will be delayed or result in variations in the type of martensite produced.

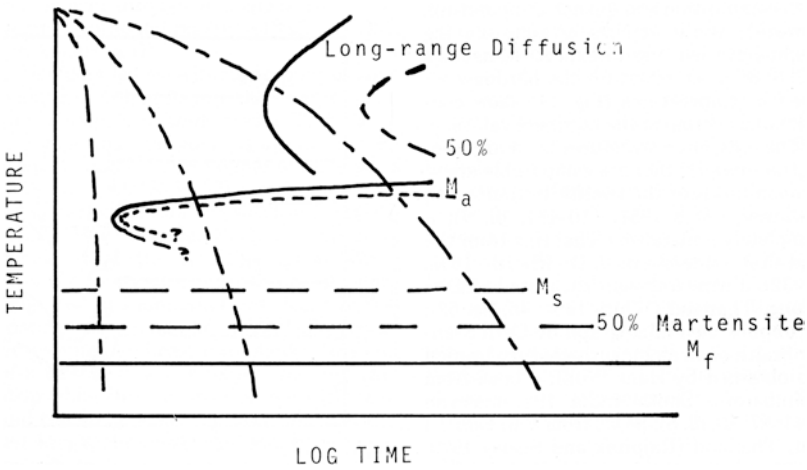

Fig. 4.49 Proposed onset and finish of martensitic transformations in the high-tin bronzes after Goodway and Conklin [32]. The chart shows that if very fast cooling takes place in the log time axis closest to the origin, then the whole structure will be martensitic. Less drastic cooling conditions will create a range of options in which the start of the martensitic transformation will be delayed or result in variations in the type of martensite produced

Probably another non-ferrous martensitic structure has been reported from copper-arsenic-antimony alloys of the Nahal Mishmar hoard [74, 106]. It has been suggested that the needle-like structure of the antimony-rich part could be of martensitic origin.

4.6.2 Diffusional Phase Transformations

4.6.2.1 Intermediate Structure: Bainite

Incomplete hardening results in the formation of one or more transformation products in addition to martensite. There are different reasons why critical cooling rates for a transformation to a principally martensitic state cannot be achieved, such as temperatures which cannot be realistically met, self-tempering, size and composition. The temperature of the red-hot steel, as well as the kind of the quenching media, the size of the object and the composition of the steel, which refers mostly to carbon, phosphorous and nickel for ancient steel, influences the hardening significantly.

The martensitic start temperatures (Ms), especially of hypoeutectoid steels, are strongly affected by their carbon contents. The transition temperatures increase with decreasing carbon content, and the incubation time for the onset of diffusion-controlled reactions is much shorter. So-called slack quenching results in the nucleation of carbide containing non-equilibrium phases such as bainite and fine lamellar pearlite, formerly known as troostite. For example, at a cooling rate of 140 °C/s, mixed structures may develop. In areas of the metal protected from the full effects of rapid quenching, the full martensitic transition cannot occur, and very dark etching nodular forms called troostite develop.

Troostite was named after the French metallurgist Louis Joseph Troost [108, p. 225] and is not resolved by the optical microscope. Therefore, troostite used to be regarded as a separate phase in its own right, although since the introduction of electron microscopy, we now know that it is a form of very fine pearlite and the term has become obsolete in metallographic nomenclature. Indeed troostite has a very distinct shape, and it is quite common in ancient iron implements where quenching has resulted in the edge or tip being hardened to martensite, but further back from this edge, troostite occurs because the rate of cooling has not been so high in this region. An example is shown in Fig. 4.50, which shows the troostite nodules in a region from a Japanese sword blade of the eighteenth century AD, further into the body of the blade, above the martensite of the cutting edge.

The high-temperature modifications of structure can get quite complex, and the region in which lath-shaped aggregates of ferrite and carbides are formed involves intermediate structures called bainite. The mechanism and characterization of bainite formation is a phenomenon which was discussed very controversially and

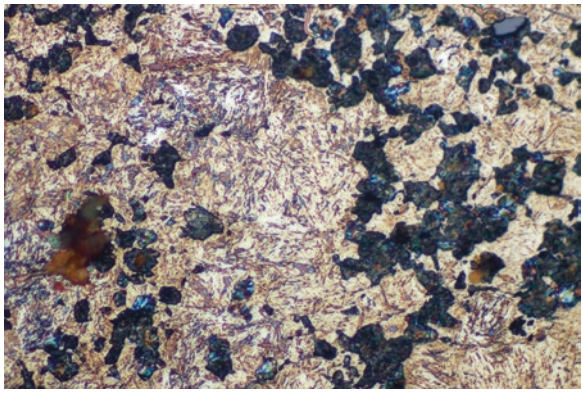

Fig. 4.50 Japanese sword blade showing the transition from martensite needles to black-blue-etching troostite as the quenching rate back from the cutting edge begins to become less. Troostite is very finely spaced pearlite nodules. Etched in nital, magnification ×430

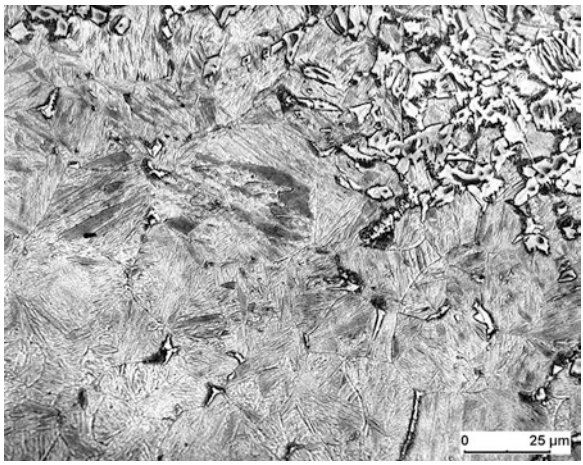

Fig. 4.51a Martensitic structure with colonies of proeutectoid ferrite of an Iron Age metalworking file from the Altburg near Bundenbach in Rhineland-Palatinate, Germany. Etched with picral

which is still in dispute [39, 97]. The microstructure was first defined by Davenport and Bain in 1930 [23] as an "intermediate appearance of dark-etching characteristics, but definitely acicular". They named it temporarily martensite-troostite, but in honour of Bain's pioneering efforts, these intermediate structures were named "bainite" by his colleagues [97]. There are large numbers of different terms and definitions for the variety of bainitic microstructures resulting from the transformation conditions and the alloying elements [39]. Two different morphologies which form in carbon steels are designated upper and lower bainite. Both can be essentially defined as a non-lamellar two-phase product of ferrite and carbides. Etching produces roughness around the carbides, and therefore bainite appears dark, compared to martensite, as seen in Figs. 4.51a and 4.51b.

The transformation to bainite is a diffusional decomposition of supersaturated austenite in which bainite is formed as aggregates of subunits of ferrite with a different nature to the carbide precipitation. Bainite formation involves lattice shear transformation, analogously to martensite as well as diffusion-controlled decomposition of austenite in its breakdown to pearlite (see Bhadeshia [2]).

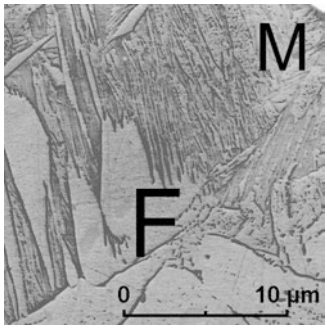

Fig. 4.51b Detail of fig. 4.51a. The inverted scanning electron micrograph shows dark etched bainite structure with carbide precipitations between ferrite (F) and martensite (M). Etched in nital

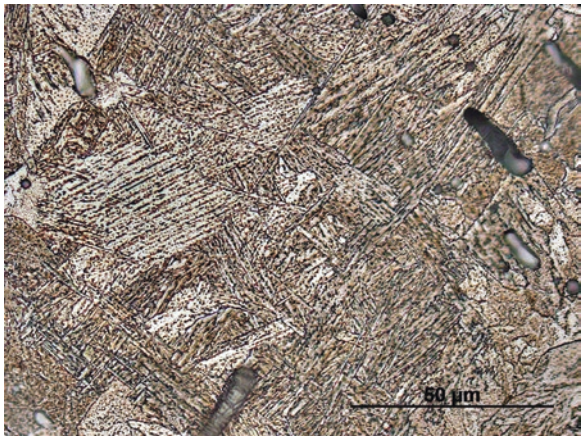

Fig. 4.52 Brown etched upper bainite in in the microstructure of another Mongolian arrowhead from a rock tomb of Nükhen Khad. Etched with Beraha's reagent I

The morphology of upper bainite, formed in the temperature range from 550 to 400 °C, is rather similar to Widmanstätten ferrite as it is composed of long ferrite laths free from internal precipitation (Fig. 4.52). Upper bainite consists of sheaves of ferrite with cementite (Fe_3C, orthorhombic) particles, which grow parallel between the ferrite plates, as shown in Fig. 4.53. In contrast to upper bainite, the carbides in lower bainite are significantly finer, and they precipitate within the plates. They are too fine and cannot be resolved in the light microscope.

The carbon has diffused to the grain boundaries, but does not form fine lamellae of ferrite and cementite, which is the case with troostite. As with Widmanstätten ferrite, the bainitic ferrite laths manifest the Kurdjumov-Sachs relationship $[(011)_\alpha \parallel (111)_\gamma]$ with the parent austenite [2]. Lower bainite that forms in the range from 400 to 250 °C appears more acicular than upper bainite, with more clearly defined individual plates assuming a lenticular habit. The most common carbide in

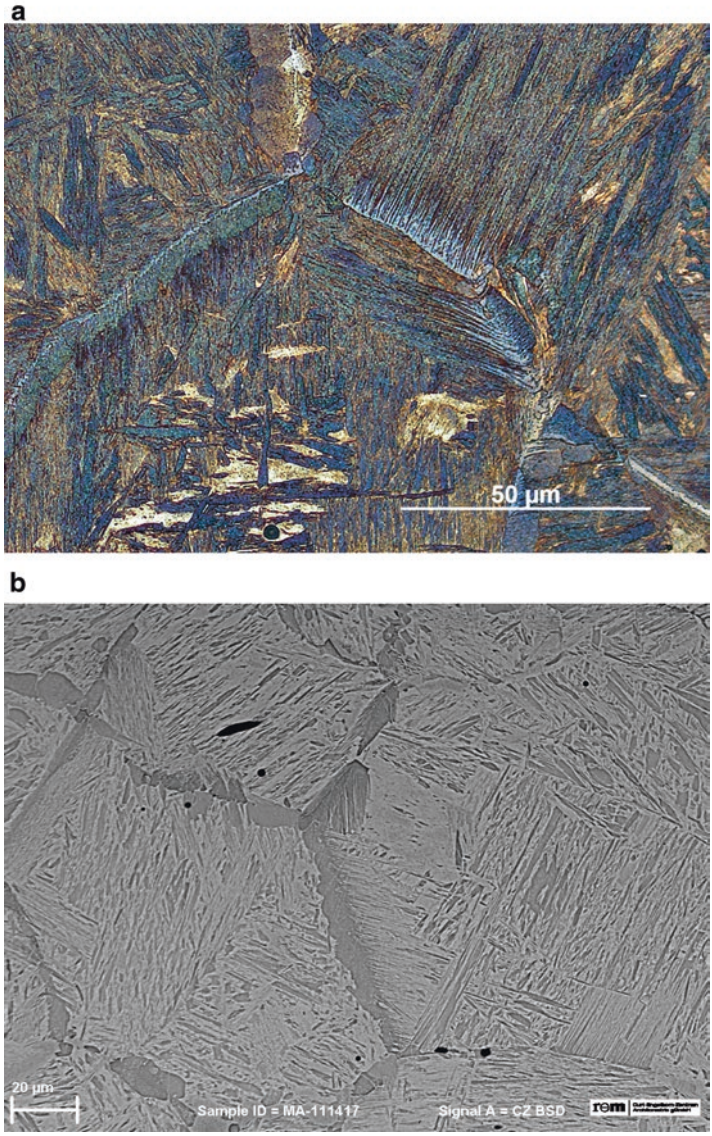

Fig. 4.53 Same arrowhead as in Fig. 4.52, but from another position and etched with sodium metabisulphite, shows lath martensite with aligned sheaves of bainite. The feathery appearance of the bainite lath is shown in the SEM image. The hardness of this arrowhead varies from 160 to 500 HV 1

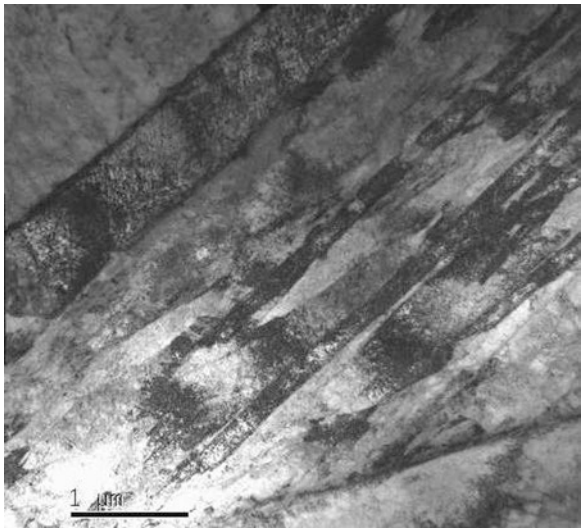

Fig. 4.54 Transmission electron bright-field micrograph from a cutting edge of a socketed axe from the Iron Age oppidum of Manching, Germany showing lower bainite plates with fine carbide precipitations

lower bainite is ε-carbide ($Fe_{3-x}C$) with a hexagonal crystal structure that forms prior to cementite [2]. The orientation relationship of ε-carbides and α_{Fe} has been determined to be:

$$011_{\alpha} \parallel 0001_{\varepsilon}$$

$$\{100\}_{\alpha} \parallel \{10\bar{1}2\}_{\varepsilon},$$

which implies a misfit $\{100\}_{\alpha}$ congruent 5° from $\{10\bar{1}2\}_{\varepsilon}$ [2].

Bainite is not frequently reported in early steels, because it is not easy to identify, as the microstructural details are so fine that their resolution is possible only using electron microscopy and only a certain volume fraction of the austenite would transform to bainite with the remainder decomposing to pearlite after an extended delay. As only small volume fractions are present in ancient iron implements, the problems associated with the identification of bainitic microstructures make the recognition in light microscopy difficult. The precipitations within quench-hardened structures can be misinterpreted as a result of the tempering of martensite, as Lang and Williams [53] have already pointed out, and confusion in nomenclature is not uncommon in the archaeometallurgical literature.

Liu et al. [57] obtained a so-called Bagaryatski orientation relationship – which is most frequently observed in bainite as well [2, 42] – between cementite precipitate and parent ferrite of the structure in prehistoric Jordanian iron objects. These results and also some needle-shaped precipitations in Roman shears are seen as effects of quench ageing [57, 76]. Quench ageing is caused by precipitation of carbides from supersaturated ferrite quenched by rapid cooling from high temperatures. Figure 4.54 shows an ion beam thinned sample of the cutting edge of a socketed axe from the Iron Age oppidum of Manching in Southern Germany.

Transmission electron micrograph reveals fine carbide precipitations within ferrite plates, and the orientation relationship between carbides and iron was determined by selected area electron diffraction to be

$$011_{\alpha} \parallel 0001_{\varepsilon}$$

$$\{100\}_{\alpha} \parallel \{10\bar{1}2\}_{\varepsilon},$$

which matches the orientation relationship of ε-carbides and α-iron in upper bainite.

4.6.2.2 Precipitation Reactions

4.6.2.2.1 Tempering of Quenched Steel

The precipitation of finely dispersed particles – very often intermetallic compounds – within the matrix strengthens and hardens some alloys, and this is purposefully used in modern non-ferrous metallurgical practice, called precipitation or age hardening. Other precipitations developed by heat treatment of metastable solid solutions do not increase but reduce hardness and increase toughness instead. This practice is best known from quench-hardened martensitic steel, which practice is called tempering.

Iron tools or weapons need to be hard but not too brittle. The high hardness and also the brittleness of martensite are based on its specific distorted structure, formed by shear, because of the supersaturation with carbon. To reduce internal stress by rearrangement of the lattice, it is necessary to reduce the carbon content by diffusion. To achieve the right degree of toughness without losing too much hardness, martensitic steels have, therefore, to be reheated after quenching, just to the right temperature. Tempering of steels occurs below the A_1 temperature, usually in the range of 200–400 °C and involves different steps of decomposition during which fine carbides precipitate (see Krauss [51]). The orientation relationship of carbides and α_{Fe} is similar to that in bainite (Sect. 4.6.2.1). There are different stages of structural change in dependence of degree of temperature to balance hardness and toughness. The blacksmith could control this by observing the colour change of the objects: because very thin iron oxide layers form, whose thickness depends on the temperature, interference colours occur. These colours which were also used as patination (e.g. “blueing”) allow a good control of the process. Rostoker and Bronson [96], using notes of Richardson from the 1880s, compiled a list of recommended temperatures/colours for a variety of tools (see Table 4.1). It shows how good tempering could be adjusted by experience to the usage of a tool, e.g. if hard or soft cast iron or wrought iron has to be cut.

Tempering of quenched iron objects has not been practiced in the European Iron Age [100] but became widespread with the Roman conquest, as it can be observed within Roman weapons [6, 25, 38]. Indeed it has not become a regular practice of Roman blacksmiths, as tools or cutlery are only sporadically tempered (see Kastowsky and Mehofer [48]; Maddin et al. [61]; Pleiner [79]; Senn Bischofberger [105]; Schaaber [99]).

Table 4.1 Compilation of recommended temperatures with corresponding colours for a variety of tools

Temperature	Colour	Tools
200 °C	Faint straw	Milling and gear tooth cutters, tools to cut hard cast iron
230 °C	Straw yellow	Dies, razors, drills for tempered saws
240 °C	"Yellow"	Pen knives, screw tops, dies, taps
250 °C	Deep straw	Taps, cutting edges of drills, chipping chisels, butchers' knives, tools to cut soft cast iron
275 °C	Bronze	Axes
290 °C	Peacock	Stone cutting chisels, springs, axes, tools to cut wrought iron
310 °C	Full blue	Drill stems, saws, tools to cut soft metals, axes
340 °C	Light blue	(needles, hacksaws, screwdrivers)
370 °C	Black	–

After Rostoker and Bronson [96: Table 1.5]

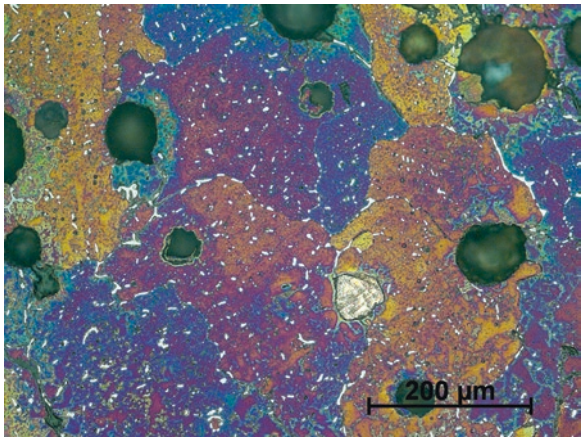

Fig. 4.55 Precipitation of intermetallic Cu_9NiSn_3 phase within a matrix of cast and annealed Drago-fibulae from the Fliess hoard, Austria. Etched with Klemm's III

4.6.2.2.2 Ageing of Copper Alloys

Quenching and tempering are practiced in several modern copper alloys, such as those containing aluminium, manganese or nickel, and also in some special brasses [24]. To our knowledge, ancient coppersmiths were not aware of ageing, but it obviously happened accidentally. It has been observed within the microstructure of a bronze brooch from the Early Iron Age (Ha C) Hoard from Fliess in Tyrol containing mean values of 14.8% tin and 2% of nickel [58]. The microstructure is still as-cast, and according to the high-tin content, the eutectoid $\alpha + \delta$ should be expected. In fact, a ternary intermetallic compound has been observed (Fig. 4.55), which is stoichiometrically related to Cu_9NiSn_3, which is labelled γ in the ternary system [17]. With reference to modern age-hardening practices of Cu-Ni-Sn alloys, it has been concluded that these precipitations result from uncontrolled ageing during solidification [58], but it could be also because of reheating the object for

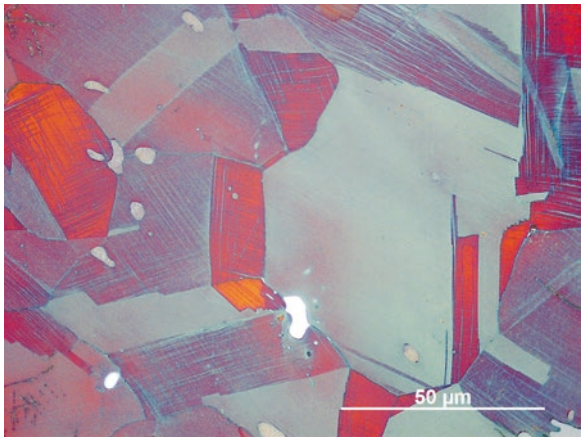

Fig. 4.56 Precipitation of intermetallic $(Cu_{1-x}Ni_x)_3Sn$ phase within a matrix of annealed and reworked α_{Cu} solid solution of a nickel-bearing bronze belt plate from Svenstrup, Denmark. Etched with Klemm's III

destruction. More recently several nickel-bearing bronzes from Denmark, dated to Nordic Bronze Age II, have been investigated and are illustrated in Fig. 4.56, which also show ternary intermetallic precipitations, which are not stoichiometrically related to Cu_9NiSn_3, but would refer to the γ'-phase $(Cu_{1-x}Ni_x)_3Sn$ (see [17]), with some amounts of arsenic and antimony, due to the fahlore origin of the copper. The microstructure of these objects are cold worked and annealed so that the ageing must have happened during annealing.

4.6.2.2.3 Ordering of Gold Alloys

Gold-copper Certain alloys will undergo an ordering reaction when annealed or even when slowly cooled. Such solid-state transformations may also cause trouble in some alloying systems, and often quenching of the alloy is used to prevent these transformations in the solid state from taking place. Gold-copper alloys, important both in ancient and historic periods, are one such system where, as can be seen from the phase diagram given above, a number of ordered phases can form. The gold-copper system is an important one, and a great deal of investigative work has been carried out. One of the first scientists who reported on this system was Roberts-Austen and Rose ([93], pp. 105–112). Pure gold melts at 1064.4 °C and copper at 1083.1 °C [126]; the equilibrium diagram, shown in Fig. 4.12, reveals that a melting minimum exists at 911 °C, corresponding to a composition of 80.1 wt.% gold and 19.9 wt.% copper.

A classic paper of 1916 by Kurnakow, Zemoznzny and Zasedatelev showed that solid-state transformations were taking place well below the eutectic temperature, and it was soon recognised that these transformations were due to ordering at certain compositions. A great deal of work has subsequently been carried out, and the nature of the ordering reactions reported in scores of papers (see Hansen and Anderko [35, p. 198]). Four reactions are well-defined; these are Cu_3Au(I), CuAu(I), CuAu(II) and $CuAu_3$.

$CuAu_3$: Between about 65 and 80 at.% gold (85–92 wt.% gold), a superlattice forms by a peritectoid transformation at about 240 °C [92].

CuAu: At about 25 at.% gold (50.8 wt.% gold), a change from the disordered face-centred cubic gold-copper solid solution occurs. There is evidence to suggest that $CuAu_3$ exists in two modifications. Scott [101] found a long period superlattice stable at about 34.0 °C, while most of the field is occupied by Cu_3Au(I), an ordered fcc structure formed from the disordered solid solution by annealing below 390 °C [20].

CuAu(I): At about 47–63 at.% gold (70–85 wt,% gold), a tetragonal superlattice forms in which alternate planes contain only copper or only gold atoms. Since the investigations of Johansson and Linde [44], the fine structure of AuCu has been extensively investigated; both long period superlattices and antiphase domains have been found of which CuAu is a classic example: CuAu(I) will form below 385 °C.

CuAu(II): Between about 385 and 410 °C, an orthorhombic superlattice will form [44], which may arise from either the disordered fcc alloy or from the tetragonal CuAu(I). It was found that, unlike normal order-disorder transformations, where the size of the ordered region is a function of the time of annealing and of the temperature at which it is carried out, the domains in CuAu(II) tend to remain the size at which they first formed. Isothermal studies of CuAu have shown [52, p. 871] that the long-period superlattice forms from the disordered alloy by slow nucleation and growth to give CuAu(I). However, CuAu(ll) grows in pyramidal plates, and in a polished section, the formation of these plates is accompanied by surface relief effects which appear to be martensitic transformations [110]. Each plate exhibits a system of fine parallel sub-bands which are twins in the orthorhombic lattice on the (101) plane. This is of interest, because some investigators have reported the existence of a martensitic transformation in ternary gold-copper-silver alloys which are probably, in fact, due to the appearance of CuAu(II).

Root ([95], p. 76) found that the hardness of copper-gold alloys, annealed above 420 °C, showed a maximum which was close to the eutectic composition. Figure 4.57 is from Rapson and Groenwald ([86], p. 38, Figure 10) and shows the variation in quenched and slow-cooled gold-copper alloy hardness values, given on the Brinell scale. For a series of conversion charts for this kind of data, see Scott [104] and Sect. 3.3.3.1.

Gold-Silver-Copper This system has also received a great deal of study, although not in as fine detail as the gold-copper system. Early work was carried out by Sterner-Rainer [114, 115] and later investigations by Hultgren and Tarnapol [40], McMullin and Norton [67] and Masing and Kloiber [69]. The ternary diagrams are shown in Figs. 4.58 and 4.59, the latter being from Rapson and Groenewald [86, p. 32], redrawn by Scott [103].

Figure 4.58 shows isothermal sections of the solidus revealing a large, two-phase field to the areas of high copper and silver content and low gold. The insolubility of copper and silver in each other and the solubility of both in gold account for the

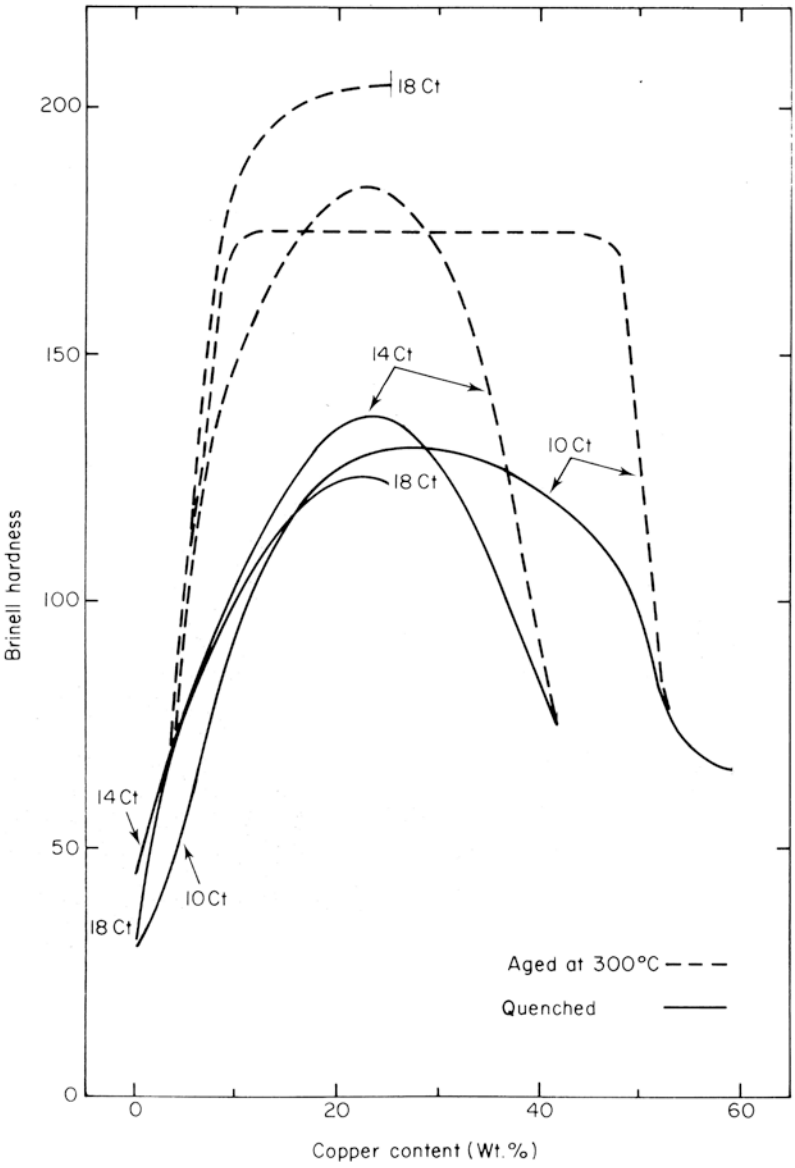

Fig. 4.57 Hardness variation on cooling or quenching of a range of gold-copper alloys

nature of the diagram in which the two-phase field becomes progressively smaller as the gold content increases. Pseudo-binary sections of the AuAgCu ternary system are shown in Fig. 4.59 and illustrate this effect of the temperature coordinates passing up the prism and composition in triangular sections.

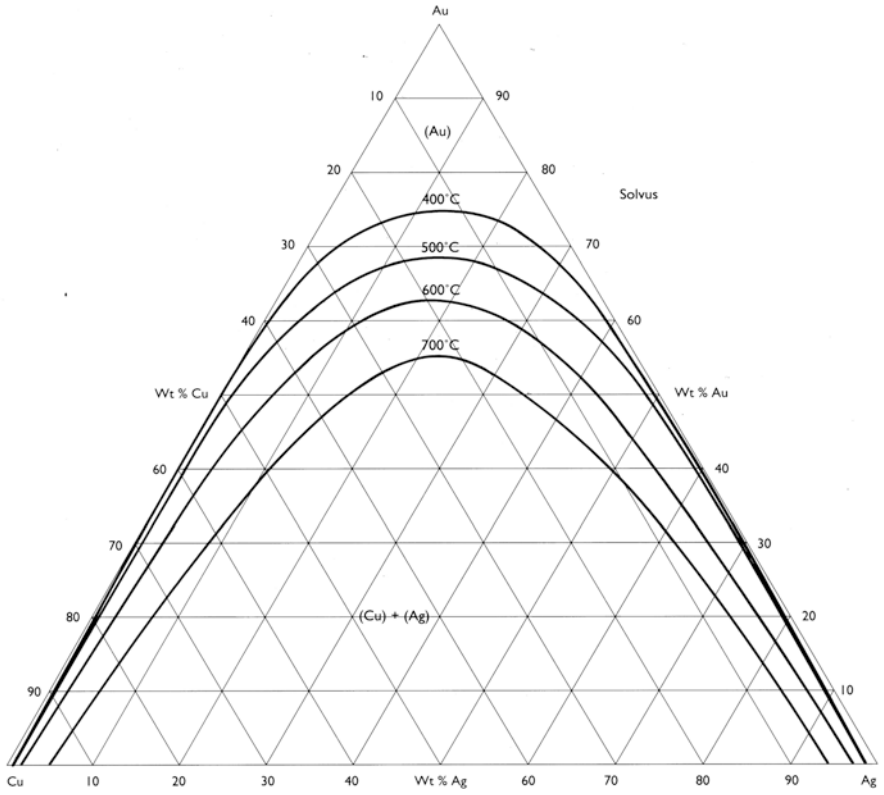

Fig. 4.58 The solidus diagram of the copper-silver-gold system, showing the miscibility gap in the solid state, which derives from the eutectic decomposition in the Ag-Cu system. (From Rapson and Groenwald [86])

The liquidus of Fig. 4.59 shows an eutectic valley half-way across the copper-silver binary extending into the gold alloys where liquidus temperatures can be as low as 850 °C. The discussion of the working properties of these alloys has been simplified by the publication of an important paper by McDonald and Sistare [66, pp. 66–73]). They define a factor f' where:

$$f' = \text{Ag wt.\%} \times 100 / \text{Ag wt.\%} + \text{Cu wt.\%}$$

By defining the gold content of the alloy to be examined and the factor f', it is possible to divide the ternary alloys into three regions based on the value of f'. For example, for 58% gold alloys (14 carat), the following regions can be defined:

Type I: f' 0–10% or from 90% to 100%. The microstructure will be that of a (AuCuAg) solid solution, and the alloys are soft in the annealed condition and cannot be age-hardened.

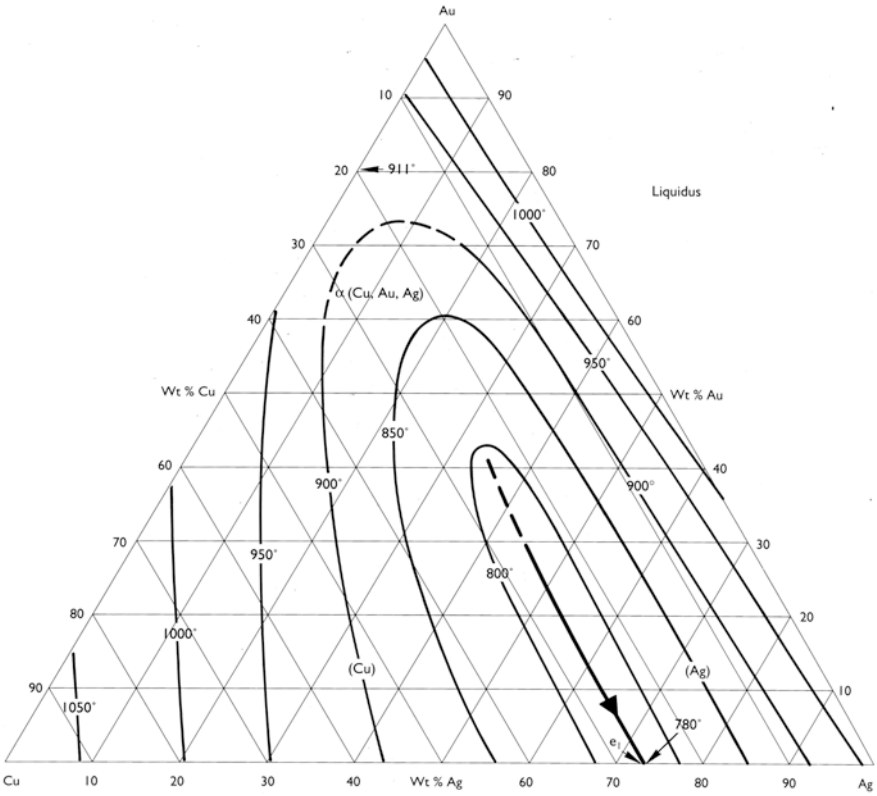

Fig. 4.59 Liquidus curves for the copper-silver-gold ternary system with the eutectic valley. (From Rapson and Groenwald [86])

Type II: *f′* 10–25% or from 75% to 90%. If cooled slowly to equilibrium at room temperature, (AgAu) will be precipitated in copper-rich alloys, while (CuAu) will be precipitated in silver-rich alloys. Type II alloys are moderately soft in the annealed state but can be age-hardened.

Type III: *f′* 25–75%. These can decompose into both (AgAu) and (CuAu). Hard in the annealed condition, difficult to quench, they can harden considerably during slow air-cooling. The colour that these alloys can show is given in the ternary colour diagram of Fig. 4.60; it can be seen that copper red occupies not only the copper corner but also most of the copper-rich and gold-rich side of the diagram. It is only at the gold-rich end of the diagram that any of the ordered phases seen in the copper-gold binary alloy appear.

McDonald and Sistare [66] only mention the existence of AuCu within the 18 carat (75 wt. % Au) gold alloys. There are then two hardening mechanisms which can occur under equilibrium conditions: ordering in high gold content alloys and precipitation hardening in a wide range of type II and type III alloys. Figure 4.57

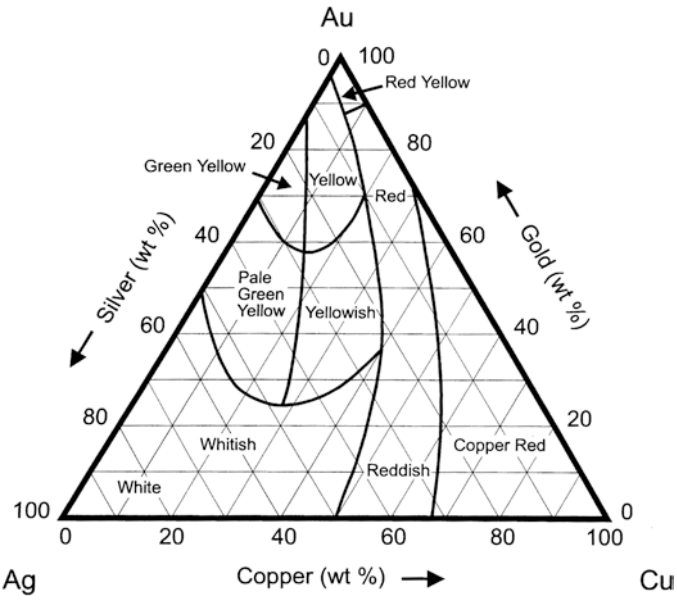

Fig. 4.60 Colour ranges for ternary gold-copper-silver alloys

shows the extent to which quenched gold-copper alloys are age-hardened and Wise [130, pp. 133–137] gives the effects of aging on various gold-silver-copper alloys. Like gold-copper alloys they also retain lower hardness values than alloys of the same composition which have been precipitation hardened by heat-treatment. The conditions under which these alloys harden are typically that of heating for 2–4 h at 205–315 °C, although some degree of hardening will also occur on cooling in air after annealing. McDonald and Sistare [66] found that annealing at 650 °C for 30 min was sufficient to recrystallize and homogenize all the alloy types. Although these alloys make very good castings, some experience is required to work them to shape by hammering and annealing operations. The ternary alloys tend to work-harden quite rapidly, and the extent to which they can be hammered without annealing is limited to 70% reduction at most.

However if annealing treatments are carried out too often, for example, if percentages reductions are less than 30%, then grain growth during annealing can be excessive and weak coarse-grained structures develop which are the cause of "orange-peel" effects on further working. These effects have been noted in the surfaces of some ancient Colombian tumbaga alloys [102].

McDonald and Sistare [66] found that quenched alloys of type I, II and III all showed homogeneous solid solution microstructures even where the slow-cooled alloys show a two-phase structure. It is interesting to note that a document of 1555 preserved in the Archive of the Indies refers to quenching as a part of Indian metal-working technology in Tamalameque, lowland Colombia [120]):

…and then the said chief and Indians burned a little charcoal on some baked clay with three cane blowpipes and placed a crucible on this with a piece of caricoli, which was brought with them, along with small quantities of low-grade gold after it had melted they took out the crucible and poured a little water over it and in this way, placing it (a bracelet) in the fire, taking it out and putting it in water and hammering it on an anvil with the stones described they worked until they had increased its size many times…

The advantages of water quenching after annealing would be to ensure that the alloy is kept in the most easily worked state before attempting to carry out further working. The preferred working method, which this document records, is definitely that of cold-working rather than hot-working. Metallurgical examination carried out in this thesis also shows that the Colombian Indians generally finished their hammering by a final process annealing. This would have been a sensible operation because many of the ternary alloys are very susceptible to stress corrosion. It is also of interest to note in this connection that Graf [33] found that the homogeneous Au-Ag-Cu alloys were more susceptible to stress corrosion cracking than that alloys of the same composition in the two-phased state.

References

1. Bachmann, H.-G.: The Identification of Slags from Archaeological Sites Institute of Archaeology Occasional Publication No. 6. Institute of Archaeology, London (1982)
2. Bhadeshia, H.K.D.H.: Bainite in Steels, 2nd edn. IOM Communications Ltd, London (2001)
3. Bhadeshia: Physical metallurgy of steels. In: Laughlin, D., Hono, K. (eds.) Physical Metallurgy III, 5th edn, pp. 2157–2214. Elsevier, Amsterdam et al. (2014)
4. Barrena, M.I., Gómez de Salazar, J.M., Soria, S.A.: Corrosion of brass archaeological blinker: characterisation of natural degradation process. Mater. Lett. **62**(24), 3944–3946 (2008)
5. Barrett, C.S., Massalski, T.B.: Structure of Metals: Crystallographic Methods, Principles and Data, International Series on Materials Science and Technology 35, 3rd rev edn. Pergamon, Oxford/New York/Seoul/Tokyo (1993)
6. Biborski, M., Kaczanowski, P., Kedzierski, Z., Stepinski, J.: Ergebnisse der metallographischen Untersuchungen römischen Schwertern aus dem Vindonissa-Museum Brugg und dem Römermuseum Augst, Jahresbericht 1985 der Gesellschaft Pro Vindonissa, pp. 45–80 (1985)
7. Breeks, J.W.: An Account of the Primitive Tribes and Monuments of the Nilagiris. Allen, London (1873)
8. Brüggler, M., Dirsch, C., Drechsler, M., Schwab, R., Willer, F.: Ein römischer Schienenarmschutz aus dem Auxiliarlager Till-Steincheshof und die Messingherstellung in der römischen Kaiserzeit. Bonner Jahrbücher. **212**, 121–152 (2012)
9. Buchwald, V.F.: Handbook of Iron Meteorites 1–3. University of California Press, Berkeley (1975)
10. Buchwald, V.F.: Ancient Iron and Slags in Greenland. Meddelelser om Grønland, Man & Society 26. Danish Polar Center, Copenhagen (2001)
11. Buchwald, V.F.: Iron and Steel in Ancient Times. Historisk-filosofiske Skrifter 29. Det Kongelige Danske Videnskabernes Selskab, Copenhagen (2005)
12. Buchwald, V.F.: Iron, Steel and Cast Iron before Bessemer. Historisk-filosofiske Skrifter 32. Det Kongelige Danske Videnskabernes Selskab, Copenhagen (2008)
13. Buchwald, V.F., Wivel, H.: Slag analysis as a method for characterization and provenancing of iron objects. Mater. Charact. **40**, 73–96 (1998)

14. Budd, P.: Alloying and metalworking in the Copper Age of Central Europe. Bull. Met. Mus. **17**, 3–14 (1992)
15. Cellini, B.: The Treatises of Benvenuto Cellini on Goldsmithing and Sculpture. Trans. C.R. Ashbee, Dover, New York (1967)
16. Chadwick, R.: The effect of composition and constitution on the working and some physical properties of the tin bronzes. J. Inst. Met. **64**, 331–346 (1939)
17. Chang, Y.A., Neumann, J.P., Mikula, A., Goldberg, D.: Phase Diagrams and Thermodynamic Properties of Ternary Copper-Metal Systems. International Copper Research Association Series on the Metallurgy of Copper 6. NSRD, Washington, DC (1979)
18. Cope, L.H.: The metallurgical analysis of Roman Imperial silver and aes coinage. In: Hall, E.T., Metcalf, D.M. (eds.) Methods of Chemical and Metallurgical Investigation of Ancient Coinage Royal Numismatic Society Special Publication 8, pp. 3–47. Royal Numismatic Society, London (1972)
19. Coustures, M.P., Béziat, D., Tollon, F., Domergue, C., Long, L., Rebiscoul, A.: The use of trace element analysis of entrapped slag inclusions to establish ore – bar iron links: examples from two Gallo-Roman iron-making sites in France (Les Martys, Montagne noire, and les Ferrys, Loiret). Archaeometry. **45**, 599–613 (2003)
20. Cowley, J.M.: X-ray measurement of order in single crystals of Cu_3Au. J. Appl. Phys. **21**(1), 24–30 (1950)
21. Craddock, P.T.: Early metal mining and production. Edinburgh University Press, Edinburgh (1995)
22. Craddock, P.T., Meeks, N.D.: Iron in ancient copper. Archaeometry. **29**(2), 187–204 (1987)
23. Davenport, E.S., Bain, E.C.: Transformation of austenite at constant subcritical temperatures. Trans. Am. Inst. Min. Metall. Eng. **90**, 117–144 (1930)
24. Davis, J.R. (ed.): ASM Specialty Handbook: Copper and Copper Alloys. ASM International, Materials Park (2008)
25. Dieudonné-Glad, N., Parisot, J.: Etude métallographique d'épées celtiques et romaines du musée Denon à Châlon-sur-Saône. In: Nicolini, G., Dieudonne-Glad, N. (eds.) Les métaux antiques: travail et restauration. Monographies Instrumentum 6, pp. 153–163. Monique Mergoil, Montagnac (1998)
26. Dillmann, P., L'Héritier, M.: Slag inclusion analyses for studying ferrous alloys employed in French medieval buildings: supply of materials and diffusion of smelting processes. J. Archaeol. Sci. **34**, 1810–1823 (2007)
27. Dillmann, P., Schwab, R., Bauvais, S., Brauns, M., Disser, A., Leroy, S., Gassmann, G., Fluzin, P.: Circulation of iron products in the North-Alpine area during the end of the First Iron Age (6th–5th c. BC): a combination of chemical and isotopic approaches. J. Archaeol. Sci. **87**, 108–124 (2017)
28. Dövener, F., Schwab, R., Willer, F.: Kleine Zeugnisse einstiger Größe – Vier Bronzestatuen-Fragmente aus Luxemburg. Archaeologia Luxemburgensis. **4**, 141–160 (2018)
29. Dungworth, D.: Serendipity in the foundry? Tin oxide inclusions in copper and copper alloys as an indicator of production process. Bull. Met. Mus. **32**, 1–5 (2000)
30. English, A.T., Chin, G.Y., Wonsiewicz, B.C.: Structures resulting from plastic deformation. In: Lyman, T. (ed.) Metallography, Structures and Phase Diagrams ASM Handbook 8, pp. 211–216. American Society for Metals, Metals Park (1973)
31. Glover, I., Bennett, A.: The high-tin bronzes of Thailand. In: Jett, P. (ed.) Scientific Research on Ancient Asian Metallurgy: Proceedings of the Fifth Forbes Symposium at the Freer Gallery of Art, pp. 101–114. Archetype, London (2012)
32. Goodway, M., Conklin, H.C.: Quenched high-tin bronzes from the Philippines. Archeomaterials. **2**, 1–27 (1987)
33. Graf, L.: The causes and mechanism of stress-corrosion cracking of homogeneous non-supersaturated alloys as derived from experimental work with alloys containing noble metal components. In: Scully, J.C. (ed.) The Theory of Stress-Corrosion Cracking in Alloys: Research Evaluation Conference Held at Ericeira, Portugal over the Period 29 March to 2 April 1971, pp. 399–341. NATO Scientific Affairs Division, Brussels (1971)

34. Hanson, D., Pell-Walpole, W.T.: Chill-Cast Tin Bronzes. Edward Arnold, London (1951)
35. Hansen, M., Anderko, K.: Constitution of Binary Alloys. McGraw-Hill, New York/Toronto/London (1958)
36. Hansen, N., Barlow, C.Y.: Plastic deformation of metals and alloys. In: Laughlin, D.E., Hono, K. (eds.) Physical Metallurgy II, 5th edn, pp. 1681–1764. Elsevier, Amsterdam et al. (2014)
37. Hauptmann, A., Maddin, R., Prange, M.: On the structure and composition of copper and tin ingots excavated from the shipwreck of Uluburun. Bull. Am. Sch. Orient. Res. **328**, 1–30 (2002)
38. Horstmann, D.: Metallkundliche Untersuchungen an Klingen von zwei römischen Dolchen Ausgrabungen und Funde in Westfalen-Lippe 9/B, pp. 111–135 (1995)
39. Hillert, M. (ed.): Viewpoint set No. 25 "bainite". Scr. Mater. **47**, 137–212 (2002)
40. Hultgren, R., Tarnapol, L.: The effect of silver on the gold-copper superlattice Au-Cu. Trans. Am. Inst. Min. Metall. Eng. **33**, 228–237 (1939)
41. Hume-Rothery, W., Raynor, G.V.: The Structure of Metals and Alloys. Institute of Metals Monograph and Report Series 1. The Institute of Metals, London (1956)
42. Illescas, F.J., Asensio, J., Guilemany, J.M.: TEM study of bainitic low-carbon HSLA steel: the orientation relationships of cementite. Pract. Metall. **44**(6), 334–346 (2007)
43. Ingo, G.M., de Caro, T., Bultrini, G.: Microchemical investigation of archaeological copper based artefacts disclosing an ancient witness of the transition from the value of the substance to the value of the appearance. Microchim. Acta. **144**(1), 87–95 (2004)
44. Johansson, C.H., Linde, J.O.: J.O.: Röntgenographische und elektrische Untersuchungen des CuAu-Systems. Ann. Phys. **417**(1), 1–48 (1936)
45. Juleff, J.: X-ray diffraction studies of gold. Unpublished BSc thesis, Institute of Archaeology, London (1981)
46. Kallfass, M., Paul, J., Jehn, H.: Investigations on the embrittlement of an antique Roman silver bowl. Practical Metallogr. **2**, 317–323 (1985)
47. Karakaya, I., Thompson, W.T.: The Ag-Sn (silver-tin) system. Bull. Alloy Phase Diagr. **8**(4), 340–347 (1987)
48. Kastowsky, K., Mehofer, M.: Metallographische Analysen an den kaiserzeitlichen Depots aus Mannersdorf am Leithagebirge. In: Pollak, M. (ed.) Stellmacherei und Landwirtschaft: zwei römische Materialhorte aus Mannersdorf am Leithagebirge, Niederösterreich. Fundberichte aus Österreich Materialhefte A 16, pp. 55–65. Berger, Wien (2006)
49. Kienlin, T.L.: Traditions and transformations: approaches to eneolithic (Copper Age) and Bronze Age metalworking and society in Eastern Central Europe and the Carpathian Basin. British Archaeological Reports International Series 2184. Archaeopress, Oxford (2010)
50. Kiessling, R.: Non-metallic Inclusions in Steel III: The Origin and Behaviour of Inclusions and their Influence on the Properties of Steels. Percy Lund, London (1968)
51. Krauss, G.: Steels: Heat Treatment and Processing Principles. ASM International, Materials Park (2000)
52. Kuczynski, G.C., Hochman, R.F., Doyama, M.: Isothermal transformations in CuAu. J. Appl. Phys. **26**, 871–874 (1955)
53. Lang, J., Williams, A.R.: The hardening of iron swords. J. Archaeol. Sci. **2**, 199–207 (1975)
54. La Niece, S.: Metallography in numismatics. In: Oddy, A., Cowell, M. (eds.) Metallurgy in Numismatics 4, Royal Numismatic Society Special Publication 30, pp. 114–133. Royal Numismatic Society, London (1998)
55. Lechtman, H.: Traditions and styles in central Andean metalwork. In: Maddin, R. (ed.) The Beginning of the Use of Metals and Alloys (BUMA I), pp. 344–378. MIT Press, Cambridge, MA (1988)
56. Lehner, J.W., Schwab, R., Pernicka, E., Schachner, A.: Cupronickel and the rise of the Hittite State: metallurgical investigations of Late Bronze Age copper alloys at Boğazköy-Hattuša (forthcoming)
57. Liu, K.H., Chan, H., Notis, M.R., Pigott, V.S.: Analytical electron microscopy of early steel from the Bacqah Valley, Jordan. In: Romig Jr., A.D., Goldstein, J.I. (eds.) Microbeam Analysis-1984, pp. 261–263. San Francisco Press, San Francisco (1984)

58. Lutz, J., Schwab, R.: The Early Iron Age hoard from Fliess in Tyrol and ore resources in the Eastern Alps. In: Pernicka, E., Schwab, R. (eds.) Under the Volcano. Forschungen zur Archäometrie und Altertumswissenschaft 5, pp. 25–34. M. Leidorf, Rahden/Westf (2014)
59. Lychatz, B.: Die Metallurgie des Rennverfahrens. Freiberger Forschungshefte D 245. Technische Universität Bergakademie Freiberg, Freiberg (2013)
60. Maddin, R.: A history of martensite: some thoughts on the early hardening of iron. In: Olson, G.B., Owen, W.S. (eds.) Martensite: A Tribute to Morris Cohen, pp. 11–19. ASM International, Materials Park (1992)
61. Maddin, R., Hauptmann, A., Baatz, D.: A metallographic examination of some iron tools from the Saalburgmuseum. Saalburg Jahrbuch. **46**, 5–23 (1991)
62. Marshall, J.: Taxila: An Illustrated Account of Archaeological Excavations Carried Out at Taxila Under the Orders of the Government of India Between the Years 1913 and 1934, vol. 1–3. Cambridge University Press, Cambridge (1951)
63. Massalski, T.B. (ed.): Binary alloy phase diagrams 1–2, Ohio. American Society of Metals, Materials Park (1986)
64. Matteoli, L., Storti, C.: Metallographic research on four pure copper axes and one related metallic block from Eneolithic Italian cave. J. Hist. Metall. Soc. **16**(2), 65–69 (1982)
65. Meeks, N.D., Tite, M.S.: The analysis of platinum-group element inclusions in gold antiquities. J. Archaeol. Sci. **7**(3), 267–275 (1980)
66. McDonald, A.S., Sistare, G.H.: The metallurgy of some carat gold jewellery alloys. Part I – coloured gold alloys. Gold Bull. **11**, 66–73 (1978)
67. McMullin, J.F., Norton, J.T.: On the structure of gold-silver-copper alloys. Trans. Am. Inst. Min. Metall. Eng. **33**, 228–237 (1949)
68. Marshall, J.: Taxila, 3 vols. Cambridge University Press, Cambridge (1951)
69. Masing, G., Kloiber, K.: Ausscheidungsvorgänge im System Kupfer-Silber-Gold. Z. Met. **32**, 125–132 (1940)
70. Melikian-Chirvani, A.S.: The white bronzes of early Islamic Iran. Metrop. Mus. J. **9**, 123–151 (1974)
71. Michalak, J.T.: Plastic deformation structures in iron and steel. In: Lyman, T. (ed.) Metallography, Structures and Phase Diagrams ASM Handbook 8, pp. 218–220. American Society for Metals, Metals Park (1973)
72. Mizutani, U., et al.: Electron theory of complex metallic alloys. In: Laughlin, D.E., Hono, K. (eds.) Physical Metallurgy I, 5th edn, pp. 103–202. Elsevier, Amsterdam et al (2014)
73. Northover, J.P.: The exploration of long-distance movement of bronze in Bronze and early Iron Age Europe. Bull. Inst. Archaeol. Univ. Lond. **19**, 45–72 (1982)
74. Northover, J.P.: Exotic alloys in antiquity. In: Rehren, T., Hauptmann, A., Muhly, J.D. (eds.) Metallurgica Antiqua. In Honour of Hans-Gert Bachmann and Robert Maddin. Der Anschnitt Beiheft 8, pp. 113–121. Deutsches Bergbau-Museum, Bochum (1998)
75. Northover, P.: Copper in the Industrial Age. In: Degrigny, C., van Langh, R., Joosten, I., Ankersmit, B. (eds.) METAL 07, vol. 1, pp. 83–90. Elsevier, Amsterdam (2007)
76. Notis, M.R., Shugar, A.N.: Roman shears: metallography, composition and historical approach to investigation. In: Archaeometallurgy in Europe 1, pp. 109–118. AIM, Milan (2003)
77. Odgen, J.: The technology of Medieval jewellery. In: Scott, D.A., Podany, J., Considine, B.B. (eds.) Ancient & Historic Metals – Conservation and Scientific Research, pp. 153–182. National Museum of Singapore, Singapore (1994)
78. Park, J.S., Park, C.W., Lee, K.J.: Implication of peritectic composition in historical high-tin bronze metallurgy. Mater. Charact. **60**(11), 1268–1275 (2009)
79. Pleiner, R.: Zur Schmiedetechnik im römerzeitlichen Bayern. Bayerische Vorgeschichtsblätter. **35**, 113–140 (1970)
80. Pleiner, R.: The Celtic Sword. Clarendon Press, Oxford (1993)
81. Pleiner, R.: Iron in Archaeology: The European Bloomery Smelters. Archeologicky Ústav Avcr, Praha (2000)

82. Pleiner, R.: Iron in Archaeology: Early European Blacksmiths. Archeologicky Ústav Avcr, Praha (2006)
83. Pliny the Elder: Natural History, 10 vols, trans. H. Rackham. Harvard University Press/ William Heinemann, Cambridge/Harvard/London (1979)
84. Pryce, O., Murillo-Barroso, M., Bellina, B., Martinón-Torres, M.: Khao Sam Kaeo – an archaeometallurgical crossroads for trans-Asiatic technological traditions. In: Srinivasan, S., Ranganathan, S., Giumlia-Mair, A. (eds.) Metals and Civilizations, Proceedings of the International Conference, Beginning of the Use of Metals and Alloys, BUMA VII, Bangalore September 2009, Bangalore, pp. 33–46 (2015)
85. Rajpitak, W., Seeley, N.: The bronze bowls from Ban Don Ta Phet: an enigma of prehistoric metallurgy. World Archaeol. **11**(1), 26–31 (1979)
86. Rapson, W.S., Groenewald, T.: Gold Usage. Academic, London (1978)
87. Ravich, I.G.: Study of the composition of Scythian and Sarmatian bronze mirrors and technologies of their manufacture. Bull. Met. Mus. **16**, 20–31 (1991)
88. Ravich, I.G., Ryndina, N.V.: Early copper-arsenic alloys and the problems of their use in the Bronze Age of the North Caucasus. Bull. Met. Mus. **23**, 1–18 (1995)
89. Reeve, M.R., Bowden, J.S., Cuthbertson, J.W.: A report on the microstructure of tin bronzes containing 15–28% tin. Part One. Met. Ind. **78**, 23–25 (1953)
90. Reeve, M.R., Bowden, J.S., Cuthbertson, J.W.: A report on the microstructure of tin bronzes containing 15-28% tin. Part Two. Met. Ind. **78**, 49–52 (1953)
91. Rehren, T., Northover, J.P.: Selenium and tellurium in ancient copper ingots. In: Pernicka, E., Wagner, G.A. (eds.) Archaeometry '90, pp. 221–228. Birkhäuser, Basel/Boston/Berlin (1991)
92. Rhines, F.N., Bond, W.E., Rummel, R.A.: Constitution of ordering alloys of the system gold-copper. Trans. Am. Soc. Met. **47**, 578–597 (1955)
93. Roberts-Austen, W.C., Rose, K.T.: On certain properties of the alloys of the gold-copper series. Proc. R. Soc. Lond. **67**(435–441), 105–112 (1901)
94. Rodney, D., Bonneville, J.: Dislocations. In: Laughlin, D.E., Hono, K. (eds.) Physical Metallurgy II, 5th edn, pp. 1591–1680. Elsevier, Amsterdam et al (2014)
95. Root, W.C.: Gold-copper alloys in ancient America. J. Chem. Educ. **28**(2), 76–78 (1951)
96. Rostoker, W., Bronson, B.: Pre-industrial Iron. Archeomaterials Monograph 1. Archeomaterials, Philadelphia (1990)
97. Samuels, L.E.: Optical Microscopy of Carbon Steels. American Society for Metals, Metals Park (1980)
98. Saunders, N., Miodownik, A.P.: The Cu-Sn (copper-tin) system. Bull. Alloy Phase Diagr. **11**(3), 278–287 (1990)
99. Schaaber, O.: Beiträge zur Frage des Norischen Eisens. Metallkundliche Grundlagen und Untersuchungen an Funden vom Magdalensberg. Carinthia I, **153**, pp. 129–279 (1963)
100. Schwab, R.: Untersuchungen zur Technologie und Herkunft eiserner Werkzeuge und Waffen. In: Sievers, S., Leicht, M., Ziegaus, B. (eds.) Ergebnisse der Ausgrabungen 1996–1999 in Manching-Altenfeld Die Ausgrabungen in Manching 18, pp. 251–293. Reichert Verlag, Wiesbaden (2013)
101. Scott, R.E.: New complex phase in the copper-gold system. J. Appl. Phys. **31**(12), 2112–2117 (1960)
102. Scott, D.A.: Pre-Hispanic Colombian metallurgy: studies of some gold and platinum alloys. PhD thesis, Institute of Archaeology, University of London (1982)
103. Scott, D.A.: Metallography and microstructure of ancient and historic metals, Getty conservation institute, J. Paul Getty Museum, Malibu (1991)
104. Scott, D.A.: Ancient Metals: Microstructure and Metallurgy 1. Conservation Science Press, Los Angeles (2011)
105. Senn Bischofberger, M.: Das Schmiedehandwerk im nordalpinen Raum von der Eisenzeit bis ins frühe Mittelalter. Internationale Archäologie – Naturwissenschaft und Technologie 5. Verlag Marie Leidorf, Rahden (2005)

106. Shalev, S., Northover, J.P.: The metallurgy of the Nahal Mishmar hoard reconsidered. Archaeometry. **35**(1), 35–47 (1993)
107. Shim, J.H., Oh, C.S., Lee, B.J., Lee, D.N.: Thermodynamic assessment of the Cu-Sn system. Z. Met. **87**, 205–212 (1996)
108. Smith, C.S.: A History of Metallography. The University of Chicago Press, Chicago (1960)
109. Smith, C.S.: Bronze technology in the east: a metallurgical study of early Thai bronzes. In: Teich, M., Young, R. (eds.) Changing Perspectives in the History of Science: Essays in Honour of Joseph Needham, pp. 21–32. Heinemann, London (1973)
110. Smith, R., Bowles, J.S.: The crystallography of the cubic to orthorhombic transformation in the alloy AuCu. Acta Metall. **8**(7), 405–415 (1960)
111. Srinivasan, S.: The use of tin and bronze in prehistoric southern Indian metallurgy. J. Met. **50**(7), 44–48 (1998)
112. Srinivasan, S., Glover, I.: Wrought and quenched, and cast high-tin bronzes in Kerala State, India. Hist. Metall. **29**(2), 69–88 (1995)
113. Srinivasan, S., Glover, I.: Skilled mirror craft of intermetallic delta high-tin bronze ($Cu_{31}Sn_8$, 32.6% tin) from Aranmula, Kerala. Curr. Sci. **93**(1), 35–40 (2007)
114. Sterner-Rainer, L.: Die Verbindung Au-Cu in Goldlegierungen. Z. Met. **17**, 162–165 (1925)
115. Sterner-Rainer, L.: Die Edelmetall-Legierungen in Industrie und Gewerbe. Verlag Wihelm Diebener, Leipzig (1930)
116. Steurer, W.: Crystal structures of metallic elements and compounds. In: Laughlin, D.E., Hono, K. (eds.) Physical Metallurgy I, 5th edn, pp. 1–101. Elsevier, Amsterdam et al (2014)
117. Stöllner, T., Oeggl, K. (eds.): Bergauf Bergab – 10.000 Jahre Bergbau in den Ostalpen. Veröffentlichung aus dem Deutschen Bergbau-Museum Bochum 207. Verlag Marie Leidorf, Bochum (2015)
118. Stöllner, T., Schwab, R.: Hart oder weich? Worauf es ankommt! Pickel aus dem prähistorischen Bergbau in den Ostalpen. Festschrift Fritz Eckart Barth, Mitteilungen der Anthropologischen Gesellschaft in Wien. **139**, 149–166 (2009)
119. Tadmor, M., Kedem, D., Begemann, F., Hauptmann, A., Pernicka, E., Schmitt-Strecker, S.: The Naḥal Mishmar hoard from the Judean Desert: technology, composition, and provenance. Atiqot. **27**, 95–148 (1995)
120. Tamalameque. Averiguaciones en Tamalameque sobre los manyllas que Mando Hazer Juan de Azpeleta a los Yndios de su Encomienda de Anpihuegas. Justicia, Legajo 610–612, folios 2520–25 (manuscript) Archivo General de Indias, Seville. Trans in Museo del Oro Archives, Bogota, Colombia (1555)
121. Uran, L.: Observations métallographiques sur les épées celtiques en fer. Revue Aquitania Supplément. **1**, 299–308 (1986)
122. Vander Voort, G.F.: Metallography, Principles and Practice. McGraw-Hill, New York (1984)
123. Voce, E.: Examination of specimens from the Pitt Rivers Museum. In: Coghlan, H.H. (ed.) Notes on the Prehistoric Metallurgy of Copper and Bronze in the Old World. Pitt Rivers Museum Occasional Papers on Technology 4, pp. 110–111. University Press, Oxford (1951)
124. Wanhill, R.J.H., Steijaart, J.P.H.M., Leenheer, R., Koens, J.F.W.: Damage assessment and preservation of an Egyptian silver vase (300–200 BC). Archaeometry. **40**(1), 123–137 (1998)
125. Wayman, M.L., Duke, M.J.M.: The effects of melting on native copper. In: Hauptmann, A., Pernicka, E., Rehren, T., Yalçın, Ü. (eds.) The Beginnings of Metallurgy. Der Anschnitt Beiheft 9, pp. 55–63. Deutsches Bergbau-Museum, Bochum (1999)
126. Weast, R.C. (ed.): The CRC Handbook of Chemistry and Physics, 59th edn. CRC Press, Boca Raton (1978)
127. Weins, W.N., Bleed, P.: Why is the Japanese sword curved? MRS Proc. **185**(p), 691–698 (1990)
128. Wheeler, T.S., Maddin, R.: The techniques of the early Thai metalsmith. Expedition. **18**(4), 38–47 (1976)
129. Willer, F., Schwab, R., Mirschenz, M.: Römische Bronzestatuen am Limes: Archäometrische Untersuchungen zur Herstellungstechnik. Bonner Jahrbücher. **216**, 57–207 (2017)

130. Wise, E.M.: Gold: Recovery, Properties, and Applications. Van Nostrand Company, Toronto/New York/London (1964)
131. Zhang, Y.M., Yang, S., Evans, J.R.G.: Revisiting Hume-Rothery's rules with artificial neural networks. Acta Mater. **56**(5), 1094–1105 (2008)
132. Zwicker, U.: Archaeometallurgical investigation on the copper – and copper-alloy-production in the area of the Mediterranean Sea (7000–1000 B.C.). Bull. Met. Mus. **15**, 3–32 (1990)